



1

2

3

4 Iron isotope insights into equatorial Pacific biogeochemistry

5

6 Authors: Capucine Camin¹, François Lacan¹, Marie Labatut¹, Catherine Pradoux¹, James W.
7 Murray²

8

9 ¹ Université de Toulouse, LEGOS (CNES/CNRS/IRD/UT), Toulouse, France

10 ² School of Oceanography, University of Washington, Seattle, Washington, USA

11

12 Corresponding authors: Capucine Camin and François Lacan, LEGOS, 14 Avenue Edouard
13 Belin, F-31400 Toulouse, France (capucine.camin@orange.fr and francois.lacan@cnrs.fr).

14

15



ABSTRACT

The EUCFe cruise (RV *Kilo Moana*, 2006) was designed to characterize sources of Fe to the western equatorial Pacific and its transport by the Equatorial Undercurrent (EUC), a narrow and fast eastward current flowing along the equator, to the eastern equatorial Pacific High Nutrient Low Chlorophyll (HNLC) region. This study presents seawater dissolved (DFe) and particulate (PFe) iron concentrations and isotopic compositions ($\delta^{56}\text{DFe}$ and $\delta^{56}\text{PFe}$) from 15 stations in the equatorial band (2°N–2°S) between Papua New Guinea and 140°W, over more than 8,500 km along the equator and in the upper 1,000 m of the water column.

$\delta^{56}\text{DFe}$ and $\delta^{56}\text{PFe}$ ranged from -0.22 to $+0.79 \pm 0.07$ ‰ and from -0.52 to $+0.43 \pm 0.07$ ‰, respectively (relative to IRMM-14, 95 % confidence interval). Source signatures, biogeochemical processes and transport all contribute to these observations. Two distinct areas, one under continental influence (the western equatorial Pacific) and an open ocean region (the central equatorial Pacific), emerged from the data. In the area under continental influence, high PFe concentrations along with $\delta^{56}\text{DFe}$ values systematically heavier than that of $\delta^{56}\text{PFe}$ indicated a permanent and reversible dissolved-particulate exchange. This exchange occurs through non-reductive processes, as previously proposed from three of the eight stations of this area (Labatut et al., 2014). In the open ocean area, preservation of a DFe isotopic signature of $\sim +0.36$ ‰ within the EUC, from Papua New Guinea to the central equatorial Pacific (7,800 km), confirmed the origin of the DFe carried within this current toward the HNLC region. At the same depth, bordering the EUC at 2°N and 2°S at 140°W, light isotopic signatures suggested that was iron originating from the eastern Pacific oxygen minimum zones. These light signatures were also observed in deeper central waters, between 200 and 500 m. Our data did not allow conclusions about fractionation during uptake by phytoplankton, but indicated that this fractionation must be if any, is small, no larger than a few tenths of a per mil.

KEY WORDS

Iron isotopes, equatorial Pacific Ocean, oxygen minimum zones, non-reductive dissolution, iron cycle, water masses.

1. INTRODUCTION

Iron (Fe) is an essential nutrient for phytoplankton, enabling them to fulfil their role as primary producers (Morel et al., 2020). Through its influence on primary productivity and plankton speciation, Fe plays a critical role in regulating the biological carbon pump and, consequently, the global carbon cycle and climate. Fe concentrations in the surface open ocean are often low (of the order of 0.1 nmol.kg^{-1}), potentially limiting primary productivity (Martin, 1992). Regions where Fe is limiting, despite the availability of macronutrients, are termed High Nutrient Low Chlorophyll (HNLC) areas. One notable HNLC region is the eastern equatorial Pacific (Chisholm and Morel, 1991), where Fe is believed to be have a main source from the western Pacific and transported eastward within the Equatorial Undercurrent (EUC) (Murray et al., 1994; Coale et al., 1996; Mackey et al., 2002; Kaupp et al., 2011). The EUC is a eastward-flowing subsurface current associated with upwellings that transports Fe from Papua New Guinea (PNG) toward South America along the equator (Gordon et al., 1997; Kaupp et al., 2011; Radic et al., 2011; Slemons et al., 2012; Winckler et al., 2016). Iron within the EUC is assumed to have both lithogenic and hydrothermal origins (Gordon et al., 1997). Specifically, the lithogenic component is suggested to primarily originate from rivers and sediments on the PNG continental margin (Mackey et al., 2002; Slemons et al., 2010; Radic et al., 2011; Labatut et al., 2014).



62 Although Fe concentration data are fundamental, isotopic measurements provide deeper
63 insight into both the provenance of Fe and internal processes governing its cycling (Lacan et
64 al., 2008; John et al., 2012; Conway and John, 2014; Ellwood et al., 2015). The isotopic
65 composition of Fe, expressed as $\delta^{56}\text{Fe}$ in per mil (‰), is defined as the deviation of the $^{56}\text{Fe}/^{54}\text{Fe}$
66 ratio of a sample from that of the IRMM-14 standard:

$$67 \quad \delta^{56}\text{Fe} = \frac{(^{56}\text{Fe}/^{54}\text{Fe})_{\text{sample}}}{(^{56}\text{Fe}/^{54}\text{Fe})_{\text{IRMM-14}}} - 1 \quad (\text{Equation 1})$$

68 The isotopic signatures can trace Fe from distinct sources, including fluvial inputs
69 (Fantle and DePaolo, 2004; Bergquist and Boyle, 2006; Ingri et al., 2006), sedimentary inputs
70 (Severmann et al., 2006; Homoky et al., 2009; Radic et al., 2011; Labatut et al., 2014),
71 hydrothermal inputs (Sharma et al., 2001; Severmann et al., 2004; Rouxel et al., 2008; Bennett
72 et al., 2009; Resing et al., 2015), and atmospheric inputs (Waeles et al., 2007; Flament et al.,
73 2008; Kurisu et al., 2016; Camin et al., 2025). They also provide information on internal oceanic
74 processes. Processes such as biological assimilation, dissolution, sorption, precipitation,
75 complexation and redox reactions, can modify the isotopic composition of Fe, through isotopic
76 fractionation.

77 Despite advances, substantial uncertainties remain regarding both the isotopic signature
78 of sources and the isotopic fractionation of processes. Hydrothermal and sedimentary sources
79 are poorly characterized due to limited understanding of the processes governing Fe exchange
80 and speciation. Additionally, the extent and mechanisms of isotopic fractionation remain
81 incompletely understood. For example, fractionation caused by phytoplankton during
82 biological uptake remains uncertain, with studies suggesting preferential uptake of either lighter
83 or heavier isotopes (Lacan et al., 2008; Radic et al., 2011; Conway and John, 2014; Ellwood et
84 al., 2015, 2020; Klar et al., 2018).

85 To better understand the sources, transport, and cycling of Fe in this region, the EUCFe
86 cruise (Equatorial Undercurrent Fe cruise) was conducted across the western and central
87 equatorial Pacific (RV Kilo Moana, PI: J. W. Murray, 2006). Iron isotope data from the EUCFe
88 cruise were previously published from four stations: three located in the west near PNG and
89 one in the open ocean (0° , 180°E) (Radic et al., 2011; Labatut et al., 2014). At the three stations
90 near PNG, an important source of dissolved Fe (DFe) was attributed to non-reductive exchange
91 processes between dissolved and mainly lithogenic particulate phases. The Fe isotope
92 signatures observed at the open ocean station indicated that in the deeper layer of the EUC the
93 Fe isotope signatures from the western Pacific were preserved toward the open ocean over more
94 than 4,000 km. The Fe isotopic composition of aerosols, collected during the cruise, was also
95 documented. Their slightly heavy signatures, $\delta^{56}\text{PFe} = +0.31 \pm 0.21$ ‰ (2SD, $n = 9$), were
96 interpreted as reflecting isotopic fractionation due to partial dissolution of crustal dust during
97 atmospheric transport (Camin et al., 2025).

98 This present study reports Fe isotopic data from an additional 11 stations from the
99 EUCFe cruise in the equatorial band (2°N - 2°S) between Papua New Guinea and 140°W , over
100 more than 8,500 km along the equator and in the top 1,000 m of the water column. By expanding
101 the spatial coverage of concentration and isotopic measurements, we constrain the basin scale
102 Fe biogeochemical cycle in the western and central equatorial Pacific.

103

104 **2. HYDRODYNAMICAL CONTEXT, WATER MASSES AND CURRENTS**

105 Seawater samples ($n=76$) were collected during the EUCFe cruise from the surface to
106 1,000 m depth in the western and central equatorial Pacific Ocean. This area is influenced by
107 the South and the North Pacific subtropical gyres that shape the large-scale circulation. The



equatorial branches of those gyres are westward currents: the North Equatorial Current (NEC) and the South Equatorial Current (SEC). The main surface and subsurface currents and the EUCFe stations with $\delta^{56}\text{Fe}$ data are represented in Figure 1.

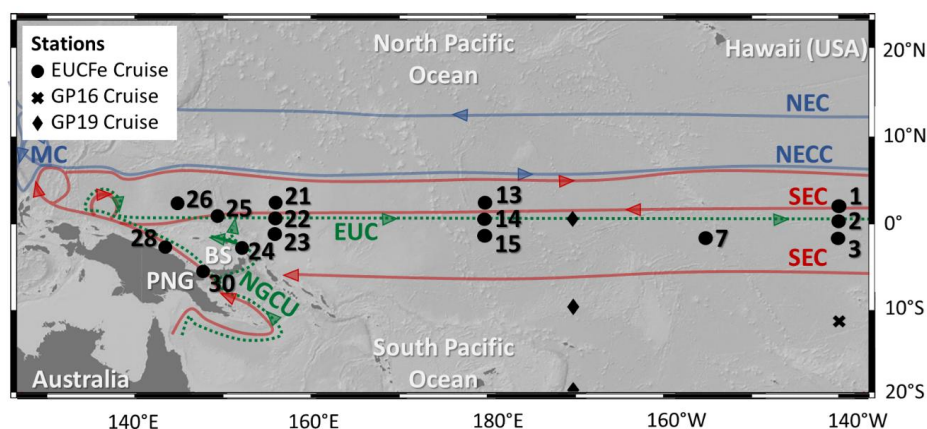
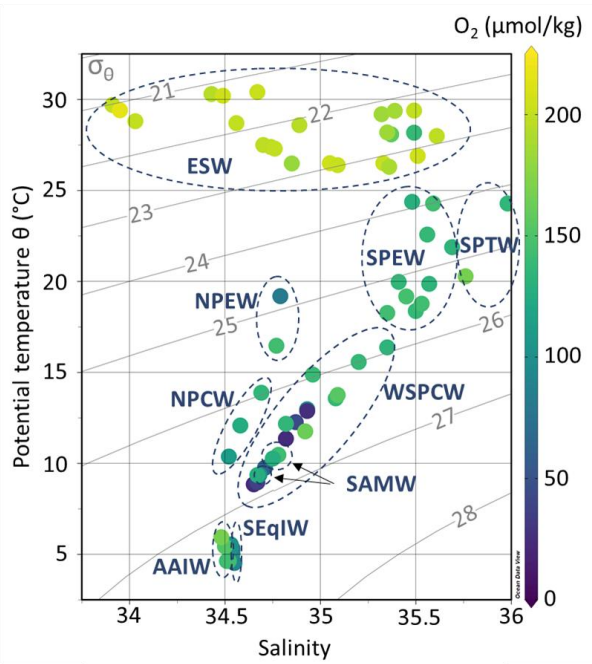


Figure 1. Map of the EUCFe stations and some GP16 and GP19 stations. Main surface and subsurface currents are represented, in blue those carrying water masses of northern origins, in red those carrying waters of southern origins and in dashed green the undercurrents. BS: Bismarck Sea; EUC: Equatorial UnderCurrent; MC: Mindanao Current; NEC: North Equatorial Current; NECC: North Equatorial CounterCurrent; NGCU: New Guinea Coastal Undercurrent; SEC: South Equatorial Current (Delcroix et al, 1992; Fine et al, 1994; Kashino et al, 1996, 2007; Johnson et al, 2002; Tomczak and Godfrey, 2003).

One of the specific structures of this circulation is the Equatorial Undercurrent (EUC). It is an intense subsurface equatorial current, with velocities up to 1 m.s^{-1} (Philander, 1973), flowing along the equator over 14,000 km (Tomczak and Godfrey, 2003). Its core rises toward the surface eastward, at an average depth of 200 m in the western equatorial Pacific, at a depth of 130 m in the central equatorial Pacific and at a depth of 40 m in the eastern equatorial Pacific (Tomczak and Godfrey, 2003; Talley et al., 2011). It is fed by waters from the Low-Latitude Western Boundary Currents (LLWBCs) composed at two-thirds by southern currents (New Guinea Coastal Current, New Guinea Coastal Undercurrent, New Ireland Coastal Undercurrent) and at one-third by northern currents (Mindanao Current) (Tsuchiya et al., 1989; Butt and Lindstrom, 1994; Fine et al., 1994; Rodgers et al., 2003; Grenier et al., 2011). The EUC is therefore enriched with nutrients of continental origins and plays an essential role supplying the eastern equatorial Pacific HNLC area through the equatorial upwelling (Coale et al., 1996; Ryan et al., 2006; Slemons et al., 2009; Kaupp et al., 2011).

Below the EUC, there is a westward subsurface flow, the Equatorial Intermediate Current (EIC). The EIC is bounded by eastward North and South Subsurface Countercurrents (NSCC and SSCC) centered around 2°N and 2°S , not shown in Figure 1 (Tomczak and Godfrey, 2003; Cravatte et al., 2017;).



137

138 Figure 2. Potential temperature (θ , $^{\circ}\text{C}$), salinity (S), dissolved oxygen concentrations (O_2 ,
139 $\mu\text{mol.kg}^{-1}$) of EUCFe samples. Isopycnals are shown in gray lines (σ_{θ} , kg.m^{-3}). The dashed
140 ellipses show water masses: Equatorial Surface Water (ESW), South Pacific Tropical Water
141 (SPTW), South Pacific Equatorial Water (SPEW), North Pacific Equatorial Water (NPEW),
142 Western South Pacific Central Water (WSPCW), North Pacific Central Water (NPCW), South
143 Antarctic Mode Water (SAMW), South Equatorial Intermediate Water (SeqIW) and Antarctic
144 Intermediate Water (AAIW).

145 Table 1. Water masses identified during the EUCFe cruise, with their characteristics in the study
146 area: origin, depth, potential temperature (θ , $^{\circ}\text{C}$), salinity, potential density anomaly (σ_{θ} , kg.m^{-3})
147 and dissolved oxygen concentration (O_2 , $\mu\text{mol.kg}^{-1}$). The currents where they flow are
148 specified. Currents acronym meanings are available in Figure 1, except for the North Equatorial
149 Subsurface Current (NESC), the South Equatorial Subsurface Current (SESC) and the New
150 Ireland Coastal Undercurrent (NICU).

151



| Water Masses | Origin | EUcFe zone | Depth (m) | θ (°C) | Salinity | σ_θ (kg m ⁻³) | O ₂ (μmol kg ⁻¹) | Currents | Characteristics | References |
|---|--|---|------------|---------------|--------------|---------------------------------------|---|---------------------------------------|--|---|
| Equatorial Surface Water (ESW) | Mixing between the Tropical Surface Water and the Subtropical upwellings, advection of the Peru Current Water | Entire zone | 0 - 100 | 21.0 - 30.5 | 33.5 - 35.7 | 20.5 - 23.5 | 108 - 193 | SEC, NGCC, NICU, EUC | / | Fiedler & Talley, 2006; EUCFe sensor data |
| South Pacific Tropical Water (SPTW) | Subduction of surface waters in the tropics in a high-salinity area (evaporation excess) around the Polynesian region | Southeastern stations (stations 3 and 15) | 100 - 200 | 18 - 25 | 35.7 - 36.7 | 24.3 - 25.3 | 134 - 167 | SEC, NGCU, NGCC, NICU, EUC | Subsurface salinity maximum | Tsuchiya et al., 1989; Qu & Lindstrom, 2002; EUCFe sensor data |
| South Pacific Equatorial Water (SPEW) | Subduction of surface waters in the tropics in a high-salinity area (evaporation excess) around the Polynesian region; one branch, less salty, of the SPTW | Mainly western equatorial and southwestern stations | 100 - 200 | 18 - 25 | 35.3 - 35.8 | 23.8 - 25.6 | 129 - 145 | SEC, NICU, NGCU, NGCC, EUC | / | Tomczak & Hao, 1989; Tsuchiya et al., 1989; Qu & Lindstrom, 2002; Tomczak & Godfrey, 2003; EUCFe sensor data |
| North Pacific Equatorial Water (NPEW) | Mixture between SPEW and NPWC | Northern stations (stations 1 and 26) | 100 - 200 | 16 - 20 | 34.7 - 35.0 | 24.3 - 25.5 | 80 - 145 | NEC, EUC | Salinity minima of tropical waters | Tomczak & Godfrey, 2003; EUCFe sensor data |
| North Pacific Central Water (NPCW) | Northern subtropical front | Northwestern stations (stations 13, 21, 26) | 200 - 300 | 10 - 17 | 33.5 - 34.7 | 25.2 - 26.4 | 110 - 135 | EUC | Salinity minima of central waters | Emery & Meincke, 1986; Pickard & Emery, 1990; Tomczak & Godfrey, 2003; Grenier, 2012; EUCFe sensor data |
| Western South Pacific Central Water (WSPCW) | Subtropical convergence zone between Tasmania and New Zealand | Equatorial and southern stations and some northern stations | 170 - 500 | 8.9 - 17 | 34.7 - 35.5 | 26.1 - 26.9 | 20 - 160 | SEC, NGCU, NICU, EUC, EIC, NSCC, SSCC | Salinity maximum of central waters | Tsuchiya, 1981; Tomczak & Hao, 1989; Tsuchiya et al., 1989; Sokolov & Rintoul, 2000; Qu & Lindstrom, 2002; Tomczak & Godfrey, 2003; Qu et al., 2009; Grenier, 2012; EUCFe sensor data |
| South Antarctic Mode Water (SAMW) | Vertical convective overturning at the end of winter north of the Antarctic Circumpolar Current | Western stations (stations 22, 24, 25) | 350 - 600 | 8.0 - 9.5 | 34.6 - 34.75 | 26.7 - 26.9 | 100 - 145 | EIC, SEC | / | McCartney, 1977; Sokolov & Rintoul, 2000; EUCFe sensor data |
| South Equatorial Intermediate Water (SEqIW) | Mixing of AAIW and Pacific Deep Water | Every sample between 700 and 1000 m depth except the Southernmost stations close to the Bismarck Sea | 700 - 1000 | 4.4 - 5.6 | 34.5 - 34.6 | 27.2 - 27.4 | 80 - 105 | EIC, NSCC, SSCC, NESCC, SESC | / | Wyrki, 1962; Bingham & Lukas, 1995; Bostock et al., 2010; EUCFe sensor data |
| AntArctic Intermediate Water (AAIW) | Subduction of fresh surface water at the subantarctic front, west of the Drake Passage | Southernmost stations in the Bismarck Sea; at less than 60 km from Papua New Guinea coast (stations 24, 28, 30) | 700 - 1000 | 4.7 - 6.0 | 34.4 - 34.6 | 27.2 - 27.3 | 140 - 170 | SEC, NGCU, NGCC, NICU | Salinity minima of intermediate waters | Tsuchiya, 1991; Tsuchiya and Talley, 1996; Talley et al., 2011; EUCFe sensor data |



152

153 In the equatorial Pacific Ocean between 140°E and 140°W, at least 9 different water
154 masses can be observed in the upper 1,000 m of the water column. Their θ , S and $[O_2]$
155 characteristics are shown in Figure 2 and reported in Table 1. The upper 100 m are mainly
156 composed of the Equatorial Surface Water (ESW), characterized by high temperatures and
157 oxygen concentrations. ESW is mainly formed from two water masses (Tropical Surface Water
158 and Subtropical Surface Water). Those are formed in the tropics where evaporation exceeds
159 precipitation and then transported toward the equator by the North and South subtropical gyres.
160 Due to mixing with upwelled waters, ESW is colder than TSW and STSW (Fiedler and Talley,
161 2006). Between 100 and 200 m, there are three water masses, from the saltiest to the freshest:
162 the South Pacific Tropical Water (SPTW), the South Pacific Equatorial Water (SPEW), the
163 North Pacific Equatorial Water (NPEW) (Tsuchiya et al., 1989; Lacan and Jeandel, 2001;
164 Grenier et al., 2013). The SPTW originates from surface waters subduction in the tropical South
165 Pacific, a high-salinity area with excess evaporation (Tsuchiya et al., 1989). The SPEW is a less
166 salty version of the SPTW and the prevailing water mass around the equator at these depths. It
167 is the major constituent of the upper part of the EUC ($\sigma_\theta < 25.6 \text{ kg.m}^{-3}$) (Lacan and Jeandel,
168 2001; Tomczak and Godfrey, 2003; Grenier et al., 2011; Grenier, 2012). The NPEW is formed
169 by mixing of the SPEW and the North Pacific Central Water (NPCW) (Tomczak and Godfrey,
170 2003). Between 200 and 500 m depth, central waters, defined by a linear region on temperature-
171 salinity diagrams, are found (Pollard et al., 1996; Stramma and England, 1999; Tomczak and
172 Godfrey, 2003). The Western South Pacific Central Water (WSPCW), formed in the subtropical
173 convergence zone between Tasmania and New Zealand, is the major constituent of the lower
174 part of the EUC ($\sigma_\theta > 25.6 \text{ kg.m}^{-3}$) (Tomczak and Hao, 1989; Grenier et al., 2011; Grenier,
175 2012;). WSPCW is also the predominant water mass at these depths in the study area. The North
176 Pacific Central Water (NPCW) is formed in the northern subtropical front (Tomczak and
177 Godfrey, 2003). NPCW is found in the northern part of the study area. Between 350 and 600
178 m, there is also the South Antarctic Mode Water (SAMW), a water mass formed by vertical
179 convective overturning at the end of the winter north of the Antarctic Circumpolar Current
180 (McCartney, 1977; Sokolov and Rintoul, 2000). The SAMW is often associated with the
181 Antarctic Intermediate Water (AAIW), a deeper water mass. Both water masses, SAMW and
182 AAIW, are found in the western part of the study area. Between 600 and 1,000 m, two
183 intermediate waters can be identified: the Equatorial Intermediate Water (EqIW) and the
184 AAIW. Some scientists refer to EqIW as part of the Antarctic Intermediate Water (AAIW)
185 (Yuan and Talley, 1992; Talley, 1999, 2008; Qu and Lindstrom, 2004). In this article, the
186 distinction between the EqIW and AAIW is relevant for studying key parameters such as
187 oxygen, nutrient concentrations and salinity along the equator. The AAIW is formed by
188 subduction of fresh surface water at the subantarctic front, west of the Drake Passage (Tsuchiya,
189 1991; Talley et al., 2011). The EqIW is a mixing of AAIW and Pacific Deep Water (formed
190 without contact with the atmosphere by Antarctic Bottom Water, Atlantic Deep Water and
191 AAIW mixing) (Tomczak and Godfrey, 2003; Bostock et al., 2010). It constitutes the
192 predominant water mass at these depths in the study region.

193

194 3. SAMPLING AND ANALYTICAL PROCEDURES

195 Sampling and analytical procedures have been previously described (Radic et al., 2011;
196 Labatut et al., 2014). They are summarized below.

197 Seawater was sampled from surface to 1,000 m depth using acid cleaned Go-Flo bottles
198 (12 L) mounted on a trace metal rosette equipped with a CTD, lent by the University of Victoria
199 (Canada). Sample filtration was performed onboard in a homemade plastic room pressurized
200 with filtered air, with acid-cleaned Nuclepore™ membranes (0.4 μm pore size, 90 mm



diameter) housed in Teflon filter holders (Savillex™). After filtration, 10 liters of filtered seawater were stored in acid-cleaned polyethylene containers and membranes were stored in acid-cleaned Petri dishes.

Samples were processed and analyzed at the LEGOS laboratory (Observatoire Midi-Pyrénées, Toulouse, France) between 2009 and 2012. All chemical procedures were conducted in a trace-metal-clean laboratory under an ISO4 laminar flow hood, using high purity reagents and acid cleaned labware.

Particles were fully digested in a mixture of 5 M HCl, 2.1 M HNO₃, and 0.6 M HF at 130 °C for 3 hours. To verify the completeness of the digestion, selected filters were re-digested, confirming no particulate Fe (PFe) remained. Leachate aliquots (2 %) were reserved for Al concentration measurements using an Element-XR HR-ICP-MS. A ⁵⁷Fe-⁵⁸Fe double spike was added to the remaining 98 % of the leachates and to filtered seawater, in preparation for isotopic analyses. Dissolved iron was preconcentrated from filtered seawater on a NTA Superflow resin, at pH = 1.8. Fe was purified from both types of samples with AG1-X4 anionic resin. Iron isotopic compositions and concentrations were measured with a Neptune MC-ICP-MS.

Uncertainties are reported at a 95 % confidence level throughout this article. For Fe concentrations and isotope measurements on the Neptune, the total procedural recovery was 93 ± 25 % for PFe and 86 ± 33 % for DFe. The total procedural blank was 0.6 % for PFe and 0.5 % for DFe of the average concentration and 9.6 % for PFe and 5.0 % for DFe of the least concentrated sample. Repeatability was 8 % for DFe concentrations, 4 % for PFe concentrations, 0.05 ‰ for δ⁵⁶DFe and 0.04 ‰ for δ⁵⁶PFe. This level of precision is better than the long-term external precision of 0.07 ‰, determined from repeated analyses of an in-house “ETH Hematite” isotopic standard. As a result, uncertainties for δ⁵⁶Fe data are reported as either ± 0.07 ‰ or the internal measurement uncertainty (2 standard errors), whichever is larger.

The LEGOS Fe isotope protocol has been validated through intercalibration and intercomparison exercises (Boyle et al., 2012; Conway et al., 2016) and detailed in Lacan et al. (2008, 2010, 2021). Accuracy (trueness and precision) of elemental concentrations measured by HR-ICP-MS was regularly verified using the certified SLRS-5 river water material and through intercalibration exercises (Yeghicheyan et al., 2013, 2019).

230

4. RESULTS

Concentrations and isotopic compositions of DFe and PFe in seawater are reported in Table 2. Previously published data from four stations (14, 24, 28 and 30) are included here for clarity (Radic et al., 2011; Labatut et al., 2014). All Fe concentrations, Fe isotopic compositions, temperature, salinity, oxygen data and an intercalibration report, have been submitted to the GEOTRACES Data Product. They are also available on the SEANOE open data repository (Lacan et al., 2025).

Table 2. Location, depth, hydrological properties, concentration and isotopic composition of dissolved and particulate Fe (DFe and PFe). Concentration relative uncertainties are 8.0 % for DFe and 4.3 % for PFe (95% confidence level). U95 stands for measurement uncertainty at the 95 % confidence level. For most samples, dissolved O₂ concentration was measured in the samples onboard. When direct measurements were not available, as indicated by the (*) symbol, oxygen concentrations from the oxygen sensor on the rosette were used following calibration with in situ data. The (+) and (°) symbols indicate data previously published by Radic et al. (2011) and Labatut et al. (2014), respectively. ESW: Equatorial Surface Water; SPTW: South Pacific Tropical Water; SPEW: South Pacific Equatorial Water; NPEW: North Pacific Equatorial Water; NPCW: North Pacific Central Water; WSPCW: Western South Pacific



248 Central Water; SAMW: South Antarctic Mode Water; SEqIW: South Equatorial Intermediate
249 Water; AAIW: Antarctic Intermediate Water; Chloro. Max: Chlorophyll Maximum layer.

250

| GoFlo bottle | Depth (m) | θ (°C) | Salinity | O ₂ ($\mu\text{mol. kg}^{-1}$) | σ_θ (kg. m^{-3}) | Water mass | DFe (nmol. kg^{-1}) | $\delta^{56}\text{DFe}$ (‰) | $\delta^{56}\text{DFe}$ U95 (‰) | PFe (nmol. kg^{-1}) | $\delta^{56}\text{PFe}$ (‰) | $\delta^{56}\text{PFe}$ U95 (‰) |
|---|--------------|------------------|----------|--|--|--------------------------|-----------------------------------|--------------------------------|---------------------------------------|-----------------------------------|--------------------------------|---------------------------------------|
| STATION 1 (1.6°N 140.0°W, cast TM3, 25 August 2006, bottom: 4364 m) | | | | | | | | | | | | |
| 12 | 15 | 26.5 | 35.05 | 204 | 22.93 | ESW | 0.26 | +0.43 | 0.08 | 0.39 | +0.06 | 0.07 |
| 10 | 48 | 26.4 | 35.09 | 202 | 22.98 | ESW (Chloro. Max.) | 0.26 | +0.32 | 0.07 | 0.43 | +0.25 | 0.07 |
| 8 | 119 | 19.2 | 34.79 | 81 | 24.82 | NPEW | 0.37 | +0.28 | 0.08 | 0.24 | +0.23 | 0.07 |
| 6 | 268 | 12.3 | 34.87 | 43 | 26.43 | WSPCW | 0.36 | -0.19 | 0.11 | 0.21 | +0.06 | 0.07 |
| 4 | 497 | 8.8 | 34.65 | ^(*) 23 | 26.88 | WSPCW | 0.71 | -0.22 | 0.09 | 0.38 | +0.12 | 0.07 |
| 2 | 794 | 5.3 | 34.54 | ^(*) 87 | 27.28 | SEqIW | 0.77 | +0.40 | 0.07 | 0.30 | -0.11 | 0.07 |
| STATION 2 (0.0°N 140.0°W, cast TM9, 26 August 2006, bottom: 4333 m) | | | | | | | | | | | | |
| 12 | 15 | 26.5 | 35.33 | 201 | 23.13 | ESW | 0.13 | +0.19 | 0.07 | 0.47 | +0.19 | 0.07 |
| 10 | 49 | 26.2 | 35.36 | 188 | 23.23 | ESW (Chloro. Max.) | 0.38 | +0.14 | 0.09 | — | — | — |
| 8 | 114 | 24.3 | 35.59 | 143 | 24.00 | SPEW | 0.17 | +0.25 | 0.07 | — | — | — |
| 6 | 246 | 13.0 | 34.93 | 98 | 26.34 | WSPCW | 0.44 | +0.29 | 0.07 | — | — | — |
| 4 | 348 | 11.4 | 34.82 | ^(*) 24 | 26.57 | WSPCW | 0.43 | -0.10 | 0.07 | — | — | — |
| 2 | 992 | 4.6 | 34.55 | ^(*) 86 | 27.37 | SEqIW | 0.61 | +0.11 | 0.07 | — | — | — |
| STATION 3 (2.0°S 139.6°W, cast TM11, 27 August 2006, bottom: 4257 m) | | | | | | | | | | | | |
| 12 | 13 | 26.9 | 35.51 | 203 | 23.13 | ESW | 0.07 | — | — | 0.60 | +0.41 | 0.07 |
| 10 | 59 | 26.9 | 35.51 | 205 | 23.14 | ESW (Chloro. Max.) | 0.06 | +0.31 | 0.07 | — | — | — |
| 8 | 110 | 20.3 | 35.76 | 167 | 25.25 | SPTW | 0.14 | +0.30 | 0.12 | 0.14 | +0.33 | 0.07 |
| 7 | 198 | 12.8 | 34.93 | 25 | 26.37 | WSPCW | 0.24 | -0.06 | 0.07 | — | — | — |
| 4 | 476 | 9.0 | 34.67 | ^(*) 36 | 26.87 | SEqIW | 0.43 | +0.14 | 0.07 | — | — | — |
| 1-2 | 993 | 4.5 | 34.55 | ^(*) 91 | 27.37 | SEqIW | 0.41 | +0.35 | 0.07 | 0.40 | +0.15 | 0.08 |
| STATION 7 (2.1°S 155.1°W, cast TM16, 02 September 2006, bottom: 4992 m) | | | | | | | | | | | | |
| 11 | 75 | 27.9 | 35.61 | 196 | 22.87 | ESW (Chloro. Max.) | 0.07 | — | — | 0.55 | +0.22 | 0.07 |
| STATION 13 (2.0°N 179.6°W, cast TM25, 10 September 2006, bottom: 5218 m) | | | | | | | | | | | | |
| 12 | 15 | 30.3 | 34.43 | 195 | 21.20 | ESW | 0.07 | +0.79 | 0.07 | 0.80 | -0.04 | 0.08 |
| 10 | 79 | 29.2 | 35.32 | 184 | 22.23 | ESW (Chloro. Max.) | 0.10 | +0.35 | 0.07 | 0.49 | +0.26 | 0.11 |
| 8 | 119 | 28.2 | 35.49 | 137 | 22.69 | ESW | 0.07 | +0.72 | 0.07 | — | — | — |
| 7 | 170 | 13.8 | 34.69 | 134 | 25.98 | NPCW | 0.32 | +0.30 | 0.08 | 0.87 | +0.12 | 0.10 |
| 4 | 377 | 10.3 | 34.75 | ^(*) 68 | 26.70 | WSPCW | 0.47 | +0.35 | 0.07 | 1.02 | +0.12 | 0.12 |
| 2 | 892 | 5.1 | 34.54 | 97 | 27.30 | SEqIW | 0.41 | +0.25 | 0.07 | 0.31 | — | — |
| STATION 14 (0.0°N 180°E, cast TM28, 11 September 2006, bottom: 5260 m) (+) | | | | | | | | | | | | |



| | | | | | | | | | | | | |
|----|-----|------|-------|-----|-------|--------------------------|------|-------|------|------|-------|------|
| 12 | 14 | 30.4 | 34.67 | 201 | 21.35 | ESW | 0.06 | — | — | 0.37 | +0.27 | 0.07 |
| 10 | 98 | 29.4 | 35.39 | 186 | 22.22 | ESW (Chloro. Max.) | 0.06 | +0.58 | 0.07 | 0.43 | +0.43 | 0.09 |
| 8 | 139 | 22.6 | 35.56 | 137 | 24.48 | SPEW | 0.20 | +0.31 | 0.08 | 0.53 | +0.13 | 0.09 |
| 6 | 197 | 14.9 | 34.86 | 140 | 25.88 | WSPCW | 0.53 | +0.40 | 0.12 | 0.53 | +0.40 | 0.07 |
| 4 | 397 | 9.8 | 34.71 | 64 | 26.76 | WSPCW | 0.61 | +0.01 | 0.07 | 0.81 | +0.15 | 0.11 |
| 2 | 842 | 5.3 | 34.54 | 82 | 27.27 | SEqIW | 0.59 | +0.22 | 0.08 | 0.51 | +0.28 | 0.10 |

STATION 15 (2.0°S 180.0°E, cast TM30, 12 September 2006, bottom: 5390 m)

| | | | | | | | | | | | | |
|----|-----|------|-------|-----|-------|--------------------------|------|-------|------|------|-------|------|
| 12 | 16 | 30.2 | 34.49 | 206 | 21.27 | ESW | 0.06 | +0.55 | 0.07 | 0.39 | +0.27 | 0.07 |
| 10 | 75 | 29.3 | 35.49 | 199 | 22.32 | ESW (Chloro. Max.) | 0.05 | — | — | 0.27 | +0.30 | 0.07 |
| 8 | 139 | 24.2 | 35.98 | 134 | 24.31 | SPTW | 0.10 | +0.43 | 0.07 | 0.33 | +0.23 | 0.12 |
| 6 | 171 | 16.4 | 35.35 | 133 | 25.93 | WSPCW | 0.23 | +0.20 | 0.07 | 0.49 | +0.12 | 0.11 |
| 2 | 844 | 5.3 | 34.53 | 99 | 27.27 | SEqIW | 0.58 | +0.32 | 0.07 | 0.98 | -0.05 | 0.10 |

STATION 21 (2.0°N 156.0°E, cast TM40, 20 September 2006, bottom: 2587 m)

| | | | | | | | | | | | | |
|----|-----|------|-------|-----|-------|--------------------------|------|-------|------|------|-------|------|
| 10 | 75 | 28.1 | 35.37 | 158 | 22.65 | ESW (Chloro. Max.) | 0.11 | — | — | 0.41 | +0.18 | 0.14 |
| 8 | 147 | 24.4 | 35.48 | 129 | 23.89 | SPEW | 0.36 | +0.40 | 0.08 | 0.60 | -0.05 | 0.07 |
| 7 | 194 | 12.0 | 34.58 | 124 | 26.25 | NPCW | 0.45 | +0.16 | 0.07 | 1.59 | +0.05 | 0.07 |

STATION 22 (0.2°N 156.0°E, cast TM43, 21 September 2006, bottom: 2049 m)

| | | | | | | | | | | | | |
|----|-----|------|-------|----------------------|-------|--------------------------|------|-------|------|------|-------|------|
| 12 | 24 | 29.7 | 33.91 | 200 | 21.00 | ESW | 0.09 | — | — | 0.39 | +0.19 | 0.07 |
| 10 | 54 | 28.6 | 34.89 | 195 | 22.12 | ESW (Chloro. Max.) | 0.09 | — | — | 0.32 | +0.22 | 0.07 |
| 8 | 191 | 18.2 | 35.35 | 143 | 25.49 | SPEW | 0.71 | +0.48 | 0.08 | 2.89 | +0.00 | 0.07 |
| 6 | 257 | 12.2 | 34.82 | 134 | 26.41 | WSPCW | 0.96 | +0.40 | 0.07 | 4.26 | +0.02 | 0.07 |
| 4 | 393 | 9.3 | 34.68 | (^c) 101 | 26.82 | SAMW | — | — | — | 1.51 | +0.01 | 0.12 |
| 3 | 393 | 9.3 | 34.68 | (^c) 101 | 26.82 | SAMW | 0.91 | +0.25 | 0.07 | 1.68 | +0.05 | 0.15 |

STATION 23 (1.2°S 155.6°E, cast TM45, 22 September 2006, bottom: 1997 m)

| | | | | | | | | | | | | |
|----|-----|------|-------|----------------------|-------|--------------------------|------|-------|------|------|-------|------|
| 10 | 74 | 28.2 | 35.35 | (^c) 183 | 22.60 | ESW (Chloro. Max.) | 0.07 | +0.26 | 0.09 | 0.29 | +0.14 | 0.11 |
| 8 | 185 | 18.4 | 35.50 | (^c) 138 | 25.56 | SPEW | 0.46 | +0.32 | 0.09 | 1.83 | -0.03 | 0.14 |
| 6 | 218 | 13.6 | 35.08 | (^c) 137 | 26.34 | WSPCW | 0.72 | +0.29 | 0.07 | 1.87 | +0.04 | 0.07 |
| 5 | 218 | 13.6 | 35.08 | (^c) 137 | 26.34 | WSPCW | 0.72 | +0.30 | 0.11 | 2.52 | -0.01 | 0.13 |
| 4 | 218 | 13.6 | 35.08 | (^c) 137 | 26.34 | WSPCW | 0.75 | +0.22 | 0.07 | 2.70 | +0.03 | 0.12 |

STATION 24 (3.2°S 152.3°E, cast TM47, 23 September 2006, bottom: 1669 m) (^c)

| | | | | | | | | | | | | |
|----|-----|------|-------|----------------------|-------|--------------------------|------|-------|------|------|-------|------|
| 11 | 39 | 28.7 | 34.56 | 199 | 21.83 | ESW | 0.48 | -0.03 | 0.07 | 1.15 | +0.13 | 0.14 |
| 9 | 64 | 27.4 | 34.74 | 196 | 22.38 | ESW (Chloro. Max.) | 0.30 | +0.20 | 0.07 | 1.66 | +0.01 | 0.16 |
| 7 | 179 | 19.9 | 35.57 | 133 | 25.22 | SPEW | 0.86 | -0.03 | 0.07 | 7.81 | -0.48 | 0.11 |
| 5 | 367 | 10.5 | 34.78 | (^c) 143 | 26.70 | WSPCW | 0.67 | +0.27 | 0.08 | 4.87 | -0.03 | 0.12 |
| 2 | 912 | 4.6 | 34.52 | 141 | 27.34 | AAIW | 0.99 | +0.34 | 0.07 | 4.91 | +0.00 | 0.10 |

STATION 25 (0°N 149.3°E, cast TM50, 25 September 2006, bottom: 3364 m)

| | | | | | | | | | | | | |
|----|-----|------|-------|-----|-------|------|------|-------|------|------|-------|------|
| 11 | 25 | 29.4 | 33.95 | 215 | 21.14 | ESW | 0.17 | — | — | 0.44 | +0.25 | 0.09 |
| 9 | 135 | 21.9 | 35.69 | 133 | 24.79 | SPEW | 0.70 | +0.03 | 0.13 | 1.44 | -0.52 | 0.10 |



| | | | | | | | | | | | | |
|---|-----|------|-------|----------------------|-------|-------|------|-------|------|------|-------|------|
| 6 | 198 | 15.6 | 35.20 | 136 | 26.00 | WSPCW | 0.75 | +0.38 | 0.14 | 4.12 | +0.02 | 0.07 |
| 5 | 372 | 10.3 | 34.75 | (^o) 126 | 26.71 | SAMW | 0.99 | — | — | 3.48 | +0.00 | 0.07 |
| 3 | 793 | 5.5 | 34.53 | (^o) 103 | 27.24 | SEqIW | 0.98 | +0.13 | 0.07 | 1.76 | -0.06 | 0.07 |
| 2 | 793 | 5.5 | 34.53 | (^o) 103 | 27.24 | SEqIW | 0.87 | — | — | 1.77 | -0.05 | 0.07 |

STATION 26 (1.6°N 145.0°E, cast TM52, 26 September 2006, bottom: 4490 m)

| | | | | | | | | | | | | |
|----|-----|------|-------|----------------------|-------|-------|------|-------|------|------|-------|------|
| 11 | 24 | 28.8 | 34.03 | 200 | 21.40 | ESW | 0.16 | — | — | 0.42 | — | — |
| 8 | 152 | 20.0 | 35.41 | 135 | 25.08 | SPEW | 0.61 | — | — | 2.20 | +0.01 | 0.07 |
| 6 | 219 | 16.4 | 34.77 | (^o) 144 | 25.48 | NPEW | 0.36 | — | — | 1.85 | +0.12 | 0.07 |
| 5 | 258 | 10.4 | 34.52 | (^o) 111 | 26.51 | NPCW | 0.64 | +0.20 | 0.07 | 2.09 | +0.04 | 0.07 |
| 3 | 346 | 9.4 | 34.67 | (^o) 127 | 26.79 | WSPCW | 0.83 | — | — | 3.76 | +0.02 | 0.07 |

STATION 28 (3.4°S 143.9°E, cast TM56, 28 September 2006, bottom: 2256 m) (+) (°)

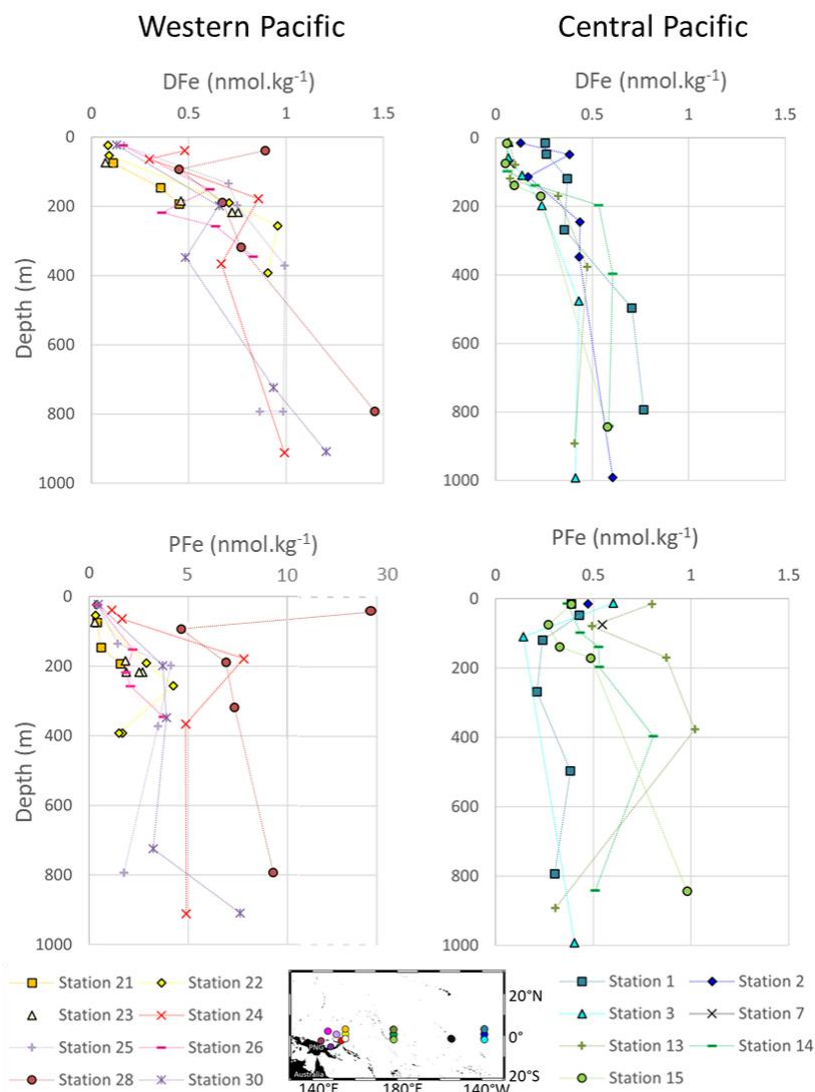
| | | | | | | | | | | | | |
|----|-----|------|-------|-------|-------|--------------------------|------|-------|------|-------|-------|------|
| 10 | 39 | 27.5 | 34.70 | 196.6 | 22.32 | ESW | 0.89 | +0.53 | 0.07 | 29.45 | +0.04 | 0.09 |
| 8 | 94 | 26.5 | 34.85 | 180.9 | 22.77 | ESW (Chloro. Max.) | 0.45 | +0.40 | 0.10 | 4.64 | +0.01 | 0.07 |
| 7 | 189 | 19.1 | 35.45 | 145 | 25.33 | SPEW | 0.67 | +0.43 | 0.11 | 6.91 | +0.29 | 0.07 |
| 5 | 319 | 13.8 | 35.09 | 154 | 26.31 | WSPCW | 0.77 | +0.29 | 0.07 | 7.34 | +0.04 | 0.07 |
| 2 | 793 | 5.5 | 34.50 | 151 | 27.22 | AAIW | 1.46 | +0.06 | 0.07 | 9.29 | -0.03 | 0.10 |

STATION 30 (5.6°S 147.4°E, cast TM61, 30 September 2006, bottom: 1040 m) (°)

| | | | | | | | | | | | | |
|----|-----|------|-------|----------------------|-------|-------|------|-------|------|------|-------|------|
| 10 | 23 | 27.3 | 34.76 | (^o) 200 | 22.44 | ESW | 0.13 | — | — | 0.45 | +0.30 | 0.11 |
| 7 | 199 | 18.7 | 35.53 | (^o) 144 | 25.49 | SPEW | 0.65 | +0.41 | 0.12 | 3.72 | +0.17 | 0.07 |
| 6 | 348 | 11.8 | 34.92 | (^o) 162 | 26.57 | WSPCW | 0.48 | +0.31 | 0.07 | 3.90 | +0.20 | 0.07 |
| 3 | 724 | 5.9 | 34.48 | (^o) 166 | 27.15 | AAIW | 0.94 | +0.44 | 0.12 | 3.23 | +0.01 | 0.07 |
| 2 | 909 | 4.6 | 34.51 | (^o) 143 | 27.33 | AAIW | 1.21 | — | — | 7.62 | -0.03 | 0.07 |

251

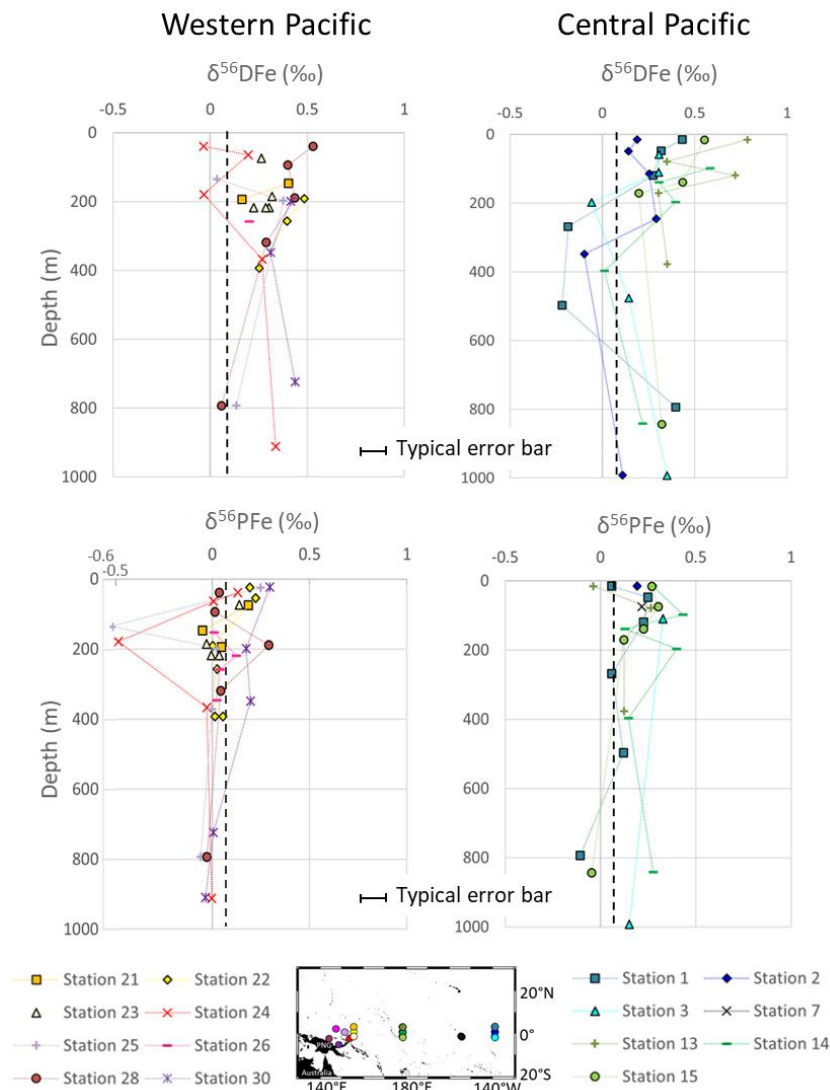
252 Two distinct groups of stations emerge from these observations. These are the western
 253 equatorial Pacific and central equatorial Pacific. In the western equatorial Pacific, PFe
 254 concentrations were significantly higher, approximately seven times larger, than typical open
 255 ocean values. This group includes stations 21, 22, 23, 24, 25, 26, 28 and 30. In the central
 256 equatorial Pacific, PFe concentrations were mostly typical of open ocean values. This group
 257 includes stations 1, 2, 3, 7, 13, 14 and 15. Data for both areas are shown in Figures 3 and 4.



258

259 Figure 3. Profiles of concentrations of DFe and PFe in nmol.kg⁻¹ in the western equatorial and
 260 central equatorial Pacific. For each station, the error bars are smaller than the symbols for Fe
 261 concentrations: on average 8 % for DFe and 4 % for PFe. Station 14 was previously published
 262 by Radic et al. (2011) and stations 24, 28 and 30 by Labatut et al. (2014). The x-axis is broken
 263 to show all PFe concentrations from western equatorial Pacific stations.

264



265

266 Figure 4. $\delta^{56}\text{DFe}$ and $\delta^{56}\text{PFe}$ profiles in the western equatorial and central equatorial Pacific.
267 The black dashed line indicates the crustal value, +0.07 ‰ (Poitrasson, 2006).

268

269 **4.1. IRON CONCENTRATIONS**

270 DFe and PFe concentrations ranged from 0.05 to 1.46 nmol.kg⁻¹ and from 0.14 to 29.45
271 nmol.kg⁻¹, respectively.

272 A few common features in Fe concentration profiles can be identified across stations
273 from the surface down to 1,000 m. i) With the exception of station 28 located near the mouth
274 of the Sepik River, lowest concentrations were found near the surface, mostly in the chlorophyll
275 maximum layer, where biological uptake depletes the concentration of bioavailable Fe. ii) From



the surface to 200 m depth, Fe concentrations tended to increase. Deeper than 200 m, the profiles became more variable, with no uniform trend across stations. iii) Stations 3, 13, 14 and 15 displayed typical open ocean, nutrient like, DFe profiles. iv) The particulate iron (PFe) fraction predominated over the dissolved fraction (DFe), accounting on average for 80 % of total iron (TFe) at western equatorial Pacific stations (140°E–156°E) and 66 % at central equatorial Pacific stations (180°E–140°W) (Figure A1).

Slemons et al. (2010, 2012) measured DFe and PFe concentrations by FIA during the same cruise. All data were of the same order of magnitude and ranged similarly. However, our data were almost systematically slightly lower (with a mean difference of $0.35 \pm 0.44 \text{ nmol.kg}^{-1}$ for DFe and $0.35 \pm 0.90 \text{ nmol.kg}^{-1}$ for PFe). In addition, EUCFe DFe and PFe concentration data are in good agreement with data published in the same area (John et al., 2018; Marsay et al., 2018; Zheng and Sohrin, 2019; Cohen et al., 2021).

4.2. IRON ISOTOPIC COMPOSITIONS

The isotopic signatures of dissolved ($\delta^{56}\text{DFe}$) and particulate Fe ($\delta^{56}\text{PFe}$) ranged from -0.22 to +0.79 ‰ and -0.52 to +0.43 ‰, respectively.

Across all stations, 85 % of the samples exhibited isotopic compositions of dissolved iron ($\delta^{56}\text{DFe}$) higher than the upper continental crust (UCC) reference value of +0.07 ‰ (Poitrasson, 2006). $\delta^{56}\text{DFe}$ of western equatorial Pacific stations ranged from -0.03 ‰ to +0.53 ‰, with an average of $+0.28 \pm 0.30 \text{ ‰}$ (2SD, $n=27$) and showed no systematic variation with depth or location. At the central equatorial Pacific stations, $\delta^{56}\text{DFe}$ ranged from -0.22 ‰ to +0.79 ‰, with an average of $+0.27 \pm 0.45 \text{ ‰}$ (2SD, $n=32$). The surface layer exhibited relatively heavy isotopic signatures (around +0.5 ‰), which generally decreased with depth, reaching values around -0.2 ‰ at approximately 400 m. Below this depth, between 800 and 1,000 m, $\delta^{56}\text{DFe}$ values increased again, to +0.4 ‰.

The isotopic compositions of particulate iron ($\delta^{56}\text{PFe}$) at the western equatorial Pacific stations, $+0.03 \pm 0.32 \text{ ‰}$ (2SD, $n=39$) on average, were remarkably homogeneous and remained close to the upper continental crust (UCC) value, except for two samples from stations 24 and 25. At the central equatorial Pacific stations, $\delta^{56}\text{PFe}$ were slightly more variable, from -0.11 to +0.43 ‰ (with an average of $+0.19 \pm 0.27 \text{ ‰}$, 2SD, $n=26$), and 81 % of the samples were heavier relative to the UCC.

EUCFe data can also be compared with two nearby cruises: GEOTRACES GP16 (2013), a zonal cruise along 10°S, from 75°W to 155°W and GEOTRACES GP19 (2015), a meridional section along 170°W with one station located at the equator (Figure 1). In the equatorial Pacific area, the circulation is highly zonal, and previous studies have shown that the water mass geochemistry at 12°S is not directly linked to that of the equatorial band (Lacan and Jeandel, 2001). This prevents the use of GP16 data and limits that of GP19 to its equatorial station (station 21). These GP19 Fe isotope data have not yet been published but are available in GEOTRACES Intermediate Data Product 2021v2 (GEOTRACES Intermediate Data Product Group, 2023). Figure 5 displays the GP19 station 21 $\delta^{56}\text{DFe}$ profile with the closest equatorial EUCFe stations, stations 2 and 14 (EUCFe station 7 is excluded from this comparison because it only reports a single data point at 75 m). Given the nine year lag between the two cruises, and the thousand km between the stations, the upper 200 m are excluded from this comparison due to potential variabilities. At four depths, approximately 200, 400, 800 and 1,000 m, $\delta^{56}\text{DFe}$ data from the two cruises can be compared (Figure 5). These are in excellent agreement. No $\delta^{56}\text{PFe}$ data have been reported for GP19.

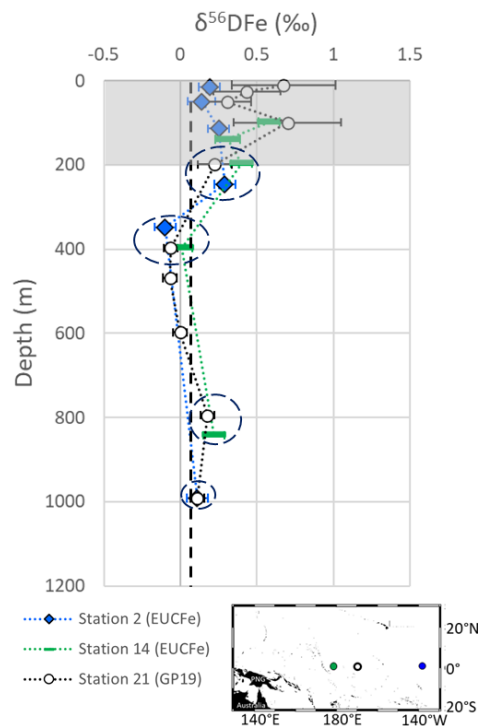


Figure 5. Comparison of $\delta^{56}\text{DFe}$ values from the EUCFe and GP19 cruises (GEOTRACES Intermediate Data Product Group, 2023). The upper 200 m, shaded in gray, are excluded from the comparison. The dashed ellipses show the 4 depths where comparison can be made for $\delta^{56}\text{DFe}$ values. The black dashed line indicates the crustal value.

5. DISCUSSION

5.1. INFLUENCE OF EXTERNAL IRON INPUTS IN THE WESTERN EQUATORIAL PACIFIC

Fe concentrations were approximately twice as high for DFe and approximately seven times higher for PFe at the western equatorial Pacific stations compared to the central equatorial Pacific stations. The particulate Fe (PFe) fraction dominated total Fe (TFe), particularly in the western equatorial Pacific stations, where PFe/TFe ratios ranged from 63 % to 97 % (Figure A1). These patterns were documented previously in several studies, and attributed to lithogenic inputs from terrestrial sources, with occasional hydrothermal contributions and minimal input from atmospheric sources (Milliman, 1995; Kineke et al., 2000; Mackey et al., 2002; Slemons et al., 2010; Radic et al., 2011; Labatut et al., 2014).

A box model was used to investigate the possible PFe sources leading to these high concentrations. It included PFe transported by oceanic currents, atmospheric deposition and delivered by rivers (notably the Sepik River, with potential deposition to and resuspension from the sediments). Particle settling within the water column and hydrothermal sources were neglected (Figure 6).



344 The transport of water masses in this area, from the surface to a depth of 1,000 m, was estimated
 345 at 18.7 Sv, based on the flow in Vitiaz Strait (Germineaud et al., 2016). The incoming water is
 346 assumed to carry a typical open ocean PFe concentration of 0.5 nmol.kg⁻¹ (Tilliette et al., 2022),
 347 prior to enrichment within the study area. The flux of PFe transported by water masses into this
 348 area, calculated as the product of these two quantities, is Flux PFe_{SW in} = 45 tons(PFe).day⁻¹.
 349 The average PFe concentration in this area (stations 21 to 30) was 3.6 nmol.kg⁻¹. This leads to
 350 a PFe flux transported out of the area by water masses, Flux PFe_{SW out} = of 326 tons(PFe).day⁻¹
 351 (3.6 nmol.kg⁻¹ multiplied by 18.7 Sv). In a steady state model, where inputs are balanced by
 352 outputs, one or more sources must be contributing approximately 281 tons(PFe).day⁻¹ to this
 353 area.

354 Particulate iron atmospheric deposition was estimated using the Fe concentration in aerosols
 355 over this region, measured during the same cruise at 3.01 ng.m⁻³ (Camin et al., 2025), multiplied
 356 by a typical aerosol deposition velocity of 1,000 m.day⁻¹ (Shelley et al., 2017). Using the
 357 deposition area shown in Figure 6, chosen as representative of this region of elevated PFe
 358 concentrations, and covering 1.6 x 10⁷ km², the resulting atmospheric PFe deposition flux was
 359 Flux PFe_{aerosol} = 49 tons(PFe).day⁻¹. This estimate accounts for only 15 % of the required
 360 external sources. Another external source to consider is sedimentary PFe flux delivered by
 361 rivers.

362 Assuming steady state, mass conservation for this model implies:

$$363 \quad \text{Flux PFe}_{\text{SW in}} + \text{Flux PFe}_{\text{aerosol}} + \text{Flux PFe}_{\text{sediment}} = \text{Flux PFe}_{\text{SW out}} \quad (\text{Equation 2})$$

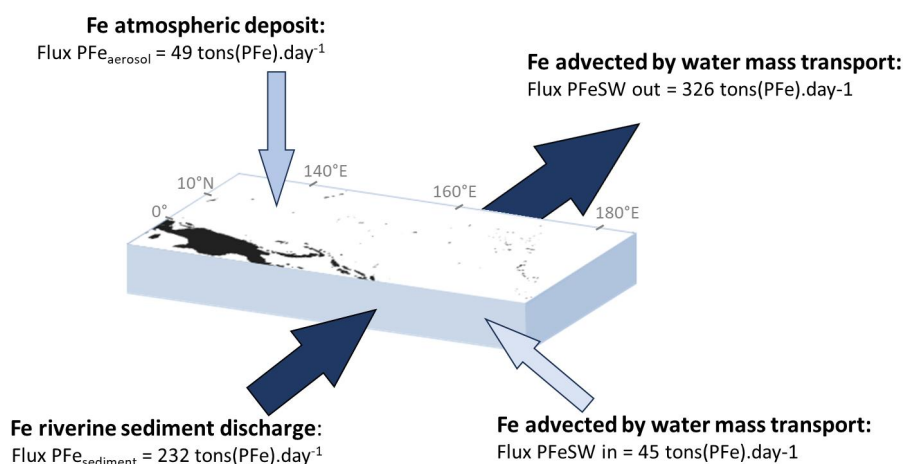
364 Taking into account the above estimates for Flux PFe_{SW in}, Flux PFe_{SW out}, and Flux PFe_{aerosol},
 365 we obtain PFe_{sediments} = 232 tons(PFe).day⁻¹, for the sedimentary PFe flux delivered by rivers
 366 and reaching the western equatorial Pacific area.

367 Papua New Guinea accounts for 8 to 10 % of the global sediment export to the ocean (1.7 x 10⁹
 368 tons(sediment).year⁻¹) (Milliman et al., 1999), with the Sepik River and other northern rivers of
 369 PNG discharging 8.6 x 10⁸ tons(sediment).year⁻¹ to this study area (Milliman et al., 1999).
 370 Assuming that Fe amounts to 5 % (w/w) of the sediment discharge, (the upper continental crust



371 (UCC) value from Rudnick and Gao, 2014), the estimated riverine discharge of PFe to the
372 western equatorial Pacific is 4.3×10^7 tons(PFe).year⁻¹, i.e., 1.2×10^5 tons(PFe).day⁻¹.

373 A very small fraction, 0.2 %, of this flux would therefore be sufficient to account for the
374 necessary 232 tons(PFe).day⁻¹. This confirms that the riverine sediment discharge is, by far, the
375 predominant source of PFe to this area.



376

377 Figure 6. Box model describing PFe inputs and output to the western equatorial Pacific region.

378 The Sepik River and other northern rivers of PNG, deliver large sediment loads to the
379 coastal ocean due to factors including intense rainfall from the Inter-Tropical Convergence
380 Zone, a narrow shelf associated with the active margin, the sediment erodibility (geology,
381 human activities) and tectonism (seismic and volcanic activity, relief) (Milliman and Syvitski,
382 1992). Lithogenic iron (Fe) observed at the western equatorial Pacific stations can be direct
383 fluvial inputs, resuspended sediments, isopycnal plumes, and hyperpycnal flows (Kineke et al.,
384 2000; Mackey et al., 2002; Kuehl et al., 2004; Renagi et al., 2010; Slemmons et al., 2010). These
385 processes can transport Fe seaward across the slope (Kineke et al., 2000; Kuehl et al., 2004;
386 Renagi et al., 2010). These lithogenic inputs, leading to very significant PFe excess compared
387 to open ocean values, extend throughout the sampled water column (0 – 1,000 m) at all stations
388 located in the western equatorial Pacific. Therefore, we discuss these data below as a whole,
389 without distinguishing between different water masses or currents.

390 At the western equatorial Pacific stations, PFe isotopic compositions are close to the
391 UCC reference value, supporting the predominantly lithogenic origin discussed above (Table 2
392 and Figure 4). Only two samples, from stations 24 and 25, exhibit near-zero $\delta^{56}\text{DFe}$ and $\delta^{56}\text{PFe}$
393 values close to -0.5 ‰, likely reflecting a hydrothermal contribution, as previously suggested
394 by Labatut et al. (2014) for station 24. Northeastern PNG is an active margin with hydrothermal
395 activity (Auzende et al., 2000) with shallow sources able to supply EUC via the NICU (Mackey
396 et al., 2002).

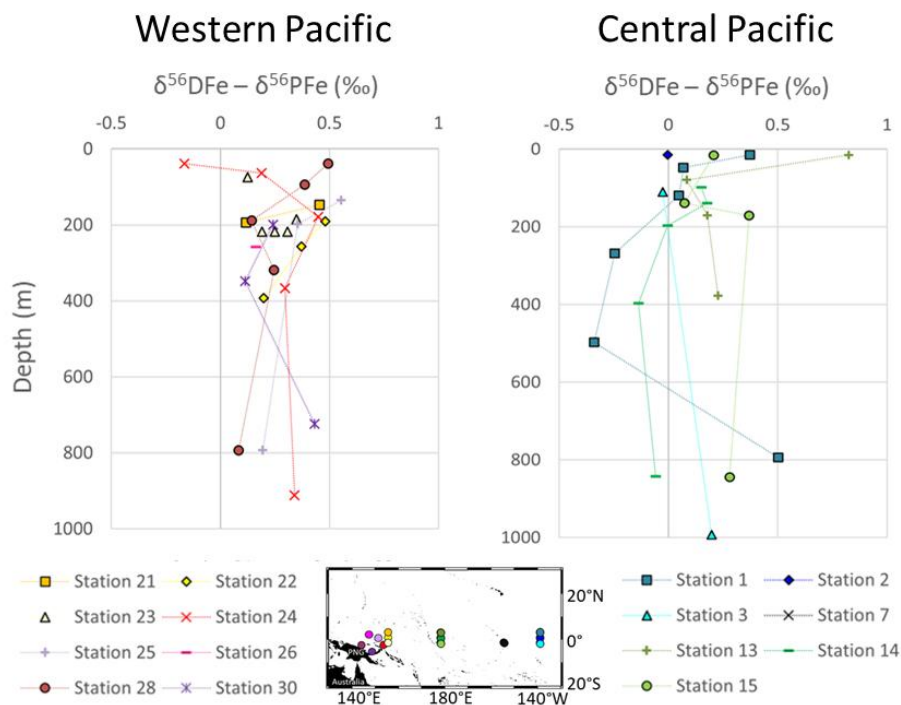
397 The isotopic difference between dissolved and particulate Fe, $\Delta^{56}\text{Fe}_{\text{DFe-PFe}}$, is shown in
398 Figure 7. Except for one data point at the surface this difference is systematically positive, i.e.,
399 DFe is systematically heavier than PFe. This is true for 26 data points out of 27, including the
400 two data points discussed above with significantly different $\delta^{56}\text{PFe}$ values (attributed to
401 hydrothermal influence). On average this difference is $\Delta^{56}\text{Fe}_{\text{DFe-PFe}} = +0.27 \pm 0.32$ ‰ (2SD,
402 n=27). This systematic difference suggests a mechanistic link between particulate and dissolved
403 Fe pools, associated to an isotopic fractionation. A kinetic isotopic fractionation associated to



404 a unidirectional reaction would lead to a reaction product isotopically lighter than the reactant.
405 In such a hypothesis, PFe being lighter than DFe, this would imply that PFe is produced from
406 DFe (for instance through precipitation). This is totally unlikely given the predominance of
407 lithogenic PFe sources in this area. We can therefore exclude the hypothesis of a kinetic
408 fractionation and conclude that there is an equilibrium isotopic fractionation between PFe and
409 DFe. Equilibrium fractionation implies co-occurrence of chemical fluxes from both phases
410 toward the other. This implies the occurrence of a permanent and reversible exchange between
411 dissolved and particulate Fe phases. In addition, because DFe is heavier than PFe, the processes
412 responsible for the flux from the particulate to the dissolved phase cannot be associated with an
413 Fe reduction process (that would have produced lighter DFe, (Criss, 1999)). This is consistent
414 with the oxygenated water column in this region (Table 2). The PFe to DFe flux is therefore a
415 non-reductive release of dissolved Fe, a process named non-reductive dissolution, NRD, by
416 Radic et al. (2011). The term NRD can refer to dissolution, as well as to other type of processes
417 from the particulate to the dissolved phase, such as desorption processes. This non-reductive
418 release of dissolved Fe probably reflects processes similar to the reversible scavenging process
419 proposed for Th or rare earth elements (REE) (Bacon and Anderson, 1982; Nozaki et al., 1987;
420 Nozaki and Alibo, 2003). These conclusions have already been proposed in previous studies
421 for stations 24, 28 and 30 (Radic et al., 2011; Labatut et al., 2014). The addition of data from
422 five additional western stations reinforces the conclusions drawn from earlier studies and
423 extends the geographic scope of these findings eastward beyond the Bismarck Sea, reaching as
424 far as 156°E. This confirms the significant role of lithogenic inputs from PNG on the
425 biogeochemistry of the area. These processes govern particulate - dissolved interactions at least
426 up to 1,200 km from the source, within the upper 1,000 m of the water column.

427 The non-reductive release of dissolved iron, NRD, at the sediment / water column
428 interface has now been observed in numerous studies as a significant external DFe source.
429 These include the western Pacific (Radic et al., 2011; Labatut et al., 2014; this study), the
430 northwest Atlantic (Conway and John, 2014), the northeast Atlantic (Klar et al., 2018), the
431 southeast Atlantic (Conway et al., 2016), the Southern Ocean (Abadie et al., 2017; Tian et al.,
432 2023) and in the southeast Pacific (John et al., 2018). In the water column, exchange fluxes
433 between particulate and dissolved phases, including non-reductive release of dissolved iron
434 from the particles, have also been proposed in several other studies (Radic et al., 2011; Abadie
435 et al., 2017; Fitzsimmons et al., 2017; John et al., 2018). In all cases, at the sediment/seawater
436 interface and within the water column, the exact processes involved remain unclear. Desorption
437 and ligand-promoted dissolution have notably been suggested (Abadie et al., 2017; John et al.,
438 2018; Homoky et al., 2021).

439



440

441 Figure 7. Differences between the dissolved and particulate of iron isotopic compositions
442 ($\delta^{56}\text{DFe} - \delta^{56}\text{PFe}$) from the surface to 1,000 m depth in the western equatorial and central
443 equatorial Pacific.

444

445 5.2. IRON SOURCES AND BIOGEOCHEMICAL DYNAMICS IN THE CENTRAL EQUATORIAL 446 PACIFIC

447 In the central equatorial Pacific region, the data are discussed within each of the five
448 density layers defined in Section 2 in order to take into account the different water masses and
449 dominant currents. Western stations are included in the figures below solely to illustrate
450 potential sources to this central Pacific area. To facilitate comparison, the $\delta^{56}\text{Fe}$ color coding is
451 the same for all density layers.

452

453 5.2.1. Surface layer, the chlorophyll maximum layer ($< 120 \text{ m}$; $< 23.8 \text{ kg.m}^{-3}$)

454

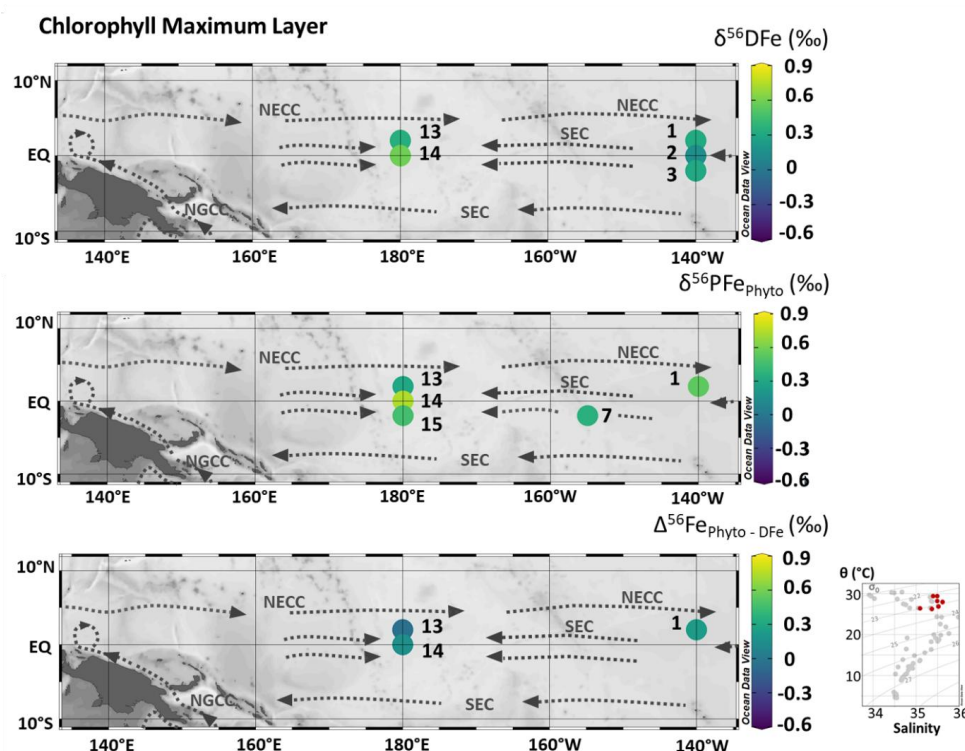


Figure 8. From the top to bottom, samples collected in the chlorophyll maximum layer, maps of $\delta^{56}\text{Df}_e$ (‰), $\delta^{56}\text{PFe}_{\text{Phyto}}$ (‰), and the difference between $\delta^{56}\text{PFe}_{\text{Phyto}}$ and $\delta^{56}\text{Df}_e$. Station numbers are displayed next to the colored dots on the map. Main currents are represented: South Equatorial Current (SEC), North Equatorial Counter Current (NECC) and New Guinea Coastal Current (NGCC). In the bottom right corner, potential temperature (θ , °C) and salinity (S) of EUCFe samples. Samples in this chlorophyll maximum layer are shown in red.

Having both dissolved and particulate iron data in the open ocean surface layer, far from continental inputs, provides an opportunity to quantify isotopic fractionation associated with biological uptake, i.e., consumption of dissolved Fe by phytoplankton and its consequent transfer to the particulate pool. We focus on the chlorophyll maximum layer (found between 10 and 100 m, based on fluorescence data shown in Figure A2), where the phytoplanktonic contribution to sampled particles is likely to be large.

Particulate iron (PFe) can originate from both authigenic or allogenetic sources. In the chlorophyll maximum layer, we assume that PFe contains both authigenic and allogenetic iron. We consider allogenetic iron to be entirely lithogenic, the predominant source of Fe in the equatorial Pacific. Assuming Aluminum (Al) is entirely lithogenic (Murray et al., 1993; Frank et al., 1995; McManus et al., 1999; Cardinal et al., 2001; Dammshäuser, 2012), the lithogenic fraction of the particulate iron, $[\text{PFe}]_{\text{lithogenic}}$, is estimated by:

$$[\text{PFe}]_{\text{lithogenic}} = [\text{PAI}]_{\text{measured}} \times \left(\frac{[\text{PFe}]}{[\text{PAI}]} \right)_{\text{reference material}} \quad (\text{Equation 3})$$

where $[\text{PAI}]_{\text{measured}}$ is the measured particulate Al concentration and $[\text{PFe}]/[\text{PAI}]_{\text{reference material}}$ is the ratio in a reference lithogenic material. Surface currents in our studied area are mainly eastward in the western Pacific and westward in the central Pacific. We therefore looked for reference lithogenic material on both the western and eastern boundaries of the Pacific basin.



479 The Fe/Al ratios of igneous rocks from the Papua New Guinea (Tiangang et al., 2024) and of
480 igneous rocks from the Galapagos Islands and the southwestern Andes basins of Peru (Wilson
481 et al., 2022; Ccanccapa-Cartagena et al., 2023) equal to 0.502 mol.mol⁻¹ and 0.499 mol.mol⁻¹
482 respectively. Given the closeness of the ratios, we utilized an average value of 0.50 mol.mol⁻¹
483 for all samples.

484 In the chlorophyll maximum layer, we found that an average of 42 % of particulate iron (PFe)
485 is lithogenic (Table A1), with the remaining 58 % attributed to authigenic sources. Assuming
486 that, in the chlorophyll maximum away from lithogenic inputs of Fe, authigenic Fe consists
487 entirely of organic Fe and furthermore of phytoplanktonic Fe (PFe_{authigenic} = PFe_{Phyto}), and
488 assuming mass conservation, $\delta^{56}\text{PFe}_{\text{Phyto}}$ can be estimated from:

$$489 \quad [\text{PFe}]_{\text{Phyto}} \cdot \delta^{56}\text{PFe}_{\text{Phyto}} \approx [\text{PFe}] \cdot \delta^{56}\text{PFe} - [\text{PFe}]_{\text{lithogenic}} \cdot \delta^{56}\text{PFe}_{\text{lithogenic}} \quad (\text{Equation 4})$$

490 where [PFe] and $\delta^{56}\text{PFe}$ are the measured particulate Fe concentration and isotopic composition.
491 The lithogenic PFe is assumed to be characterized by average crustal signature $\delta^{56}\text{PFe}_{\text{lithogenic}} =$
492 $+0.07 \pm 0.02 \text{ ‰}$ (Poitrasson, 2006). The estimated isotope compositions of phytoplanktonic
493 PFe are shown in Figure 8 and Table A1. $\delta^{56}\text{PFe}_{\text{Phyto}}$ varies from $+0.30 \pm 0.12 \text{ ‰}$ to
494 $+0.73 \pm 0.17 \text{ ‰}$. Propagation of uncertainties for Fe and Al concentrations and Fe isotopes in
495 both the samples and the reference material implies uncertainties for $\delta^{56}\text{PFe}_{\text{Phyto}}$ significantly
496 higher than those of our initial data.

497 At three stations, the isotope data are available for both the dissolved and the
498 phytoplanktonic iron. This allows an estimate of isotope fractionation associated with
499 phytoplankton uptake. Assuming two simple isotopic models, either an equilibrium
500 fractionation model (implying bidirectional chemical reactions) or a kinetic fractionation model
501 in which phytoplankton is the instantaneous product of DFe (implying unidirectional chemical
502 reactions), the isotopic fractionation can be calculated, with the same simple equation (Hayes,
503 2004):

$$504 \quad \Delta^{56}\text{Fe}_{\text{Phyto-DFe}} = \delta^{56}\text{PFe}_{\text{Phyto}} - \delta^{56}\text{DFe} \quad (\text{Equation 5})$$

505 This leads to $\Delta^{56}\text{Fe}_{\text{Phyto-DFe}} = +0.22 \pm 0.21 \text{ ‰}$ at station 1, $-0.05 \pm 0.14 \text{ ‰}$ at station 13 and
506 $+0.15 \pm 0.19 \text{ ‰}$ at station 14, with a grand average value of $\Delta^{56}\text{Fe}_{\text{Phyto-DFe}} = +0.11 \pm 0.28 \text{ ‰}$
507 (2SD, n=3) (Figures 8 and Table A1). Given the uncertainties, we cannot conclude that there is
508 isotopic fractionation associated with biological uptake, but our data indicate that if it exists, it
509 is small and lies between -0.17 and $+0.39 \text{ ‰}$ ($+0.11 \pm 0.28$) at a 95% confidence level.

510 These results can be compared with previous studies. Some suggest preferential uptake
511 of light and others of heavy isotopes. From the same cruise, Radic et al. (2011) found
512 $\Delta^{56}\text{Fe}_{\text{Phyto-DFe}} = -0.25 \pm 0.10 \text{ ‰}$ (2SD) with one model and $-0.13 \pm 0.11 \text{ ‰}$ (2SD) with a second
513 model. While the first model was based solely on DFe data, the second incorporated PFe data
514 assuming PFe was exclusively phytoplanktonic, whereas our results indicate a substantial
515 lithogenic contribution at the open ocean stations (Table A1). Off New Zealand, during the
516 annual spring bloom, Ellwood et al. (2015) estimated an isotopic fractionation of -0.54 ‰ . In
517 this work the isotopic signatures of the particles were used, but not corrected for their lithogenic
518 fractions, despite proximity to the mainland, and fractionation uncertainties were not discussed.
519 In two Antarctic coastal polynyas, preferential uptake of light isotopes have been suggested
520 based on water mass DFe signatures alone (without PFe data), with isotopic fractionation of -1
521 ‰ ($\alpha = \delta^{56}\text{Fe}_{\text{Biomass}} / \delta^{56}\text{Fe}_{\text{Seawater}} = 0.999$) (Sieber et al., 2021) and of -1.8 to -1 ‰ ($\alpha = 0.9982$
522 to 0.9990) (Tian et al., 2023). However, both studies highlighted the co-occurrence of multiple
523 mechanisms and, therefore, of several isotopic fractionation processes in the surface layer.
524 Ellwood et al. (2020) conducted a study using both DFe and PFe isotope data in a 1-D model,
525 and found isotopic fractionation values for biological uptake ranging from -1 ‰ (in a simplified
526 model considering only biological uptake) to -0.6 ‰ when using a more sophisticated model



representing additional processes (regeneration, scavenging and complexation) in a cold-core eddy in the Southern Ocean. Again, fractionation uncertainties were not discussed in these three studies. Finally, in the North Atlantic, two studies suggested a positive fractionation (contrasting with the previous studies) based on water mass DFe signatures (no PFe data) and without quantification (Conway and John, 2014; Klar et al., 2018).

The above differences may reflect regional variabilities, including differences in phytoplankton community, as well as differences in methodology such as the use of particulate data. The present analysis does not allow us to draw conclusions regarding a preferential uptake of heavy or light iron isotopes during biological uptake. However, our results confirm that this fractionation is small, likely not larger than a few tenths of a per mil. They align with a former study, in the Southern Ocean, where fractionation was quantified with a small amplitude, $|\Delta^{56}\text{Fe}_{\text{Phyto-DFe}}| < 0.32 \text{ ‰}$, with no conclusion about the direction (Lacan et al., 2008). Our analysis emphasizes the importance of taking into account error propagations and lithogenic contributions to the particulate phases, even in the chlorophyll maximum in the open ocean.

541

5.2.2. Subsurface layer (110 – 220 m; 23.8 – 25.6 kg.m⁻³), upper EUC

543

544

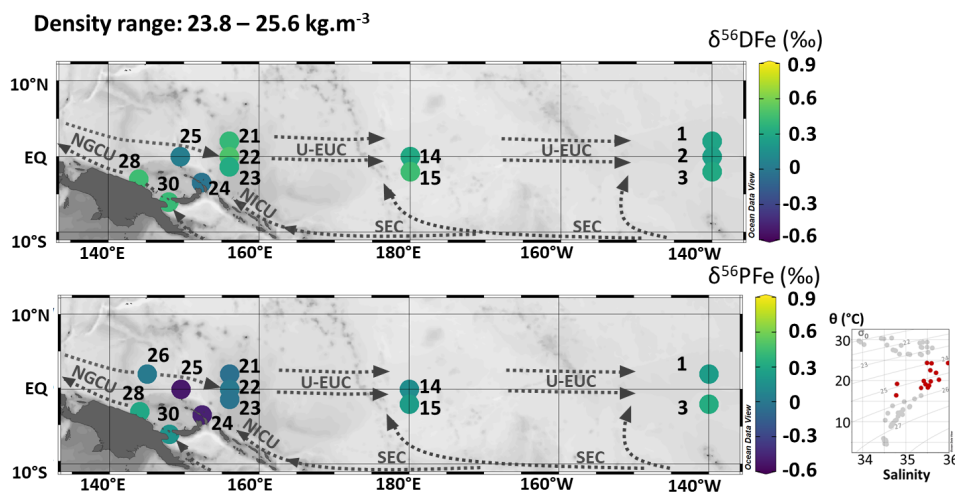


Figure 9. Map of dissolved ($\delta^{56}\text{DFe}$) and particulate ($\delta^{56}\text{PFe}$) iron isotopes for samples with potential densities between 23.8 and 25.6 kg.m⁻³. Station numbers are displayed next to the colored dots. Main currents are represented: the upper Equatorial Undercurrent (U-EUC), the South Equatorial Current (SEC), the New Guinea Coastal Undercurrent (NGCU) and the New Ireland Coastal Undercurrent (NICU). In the bottom right corner, potential temperature (θ , °C) and salinity (S) of EUCFe samples. Samples in this density layer are shown in red.

The subsurface layer is composed of three water masses: the South Pacific Tropical Water (SPTW) (stations 3 and 15), the South Pacific Equatorial Water (SPEW) (stations 2, 14, 21, 22, 23, 24, 25, 28 and 30) and the North Pacific Equatorial Water (NPEW) (stations 1 and 26) (Figure 9). At the equator, seawater within SPEW is subject to substantial renewal as it flows eastward from the western Pacific (140°E) to the central equatorial Pacific (140°W) (Tsuchiya et al., 1989; Grenier et al., 2011). This renewal is largely driven by equatorial upwelling which creates divergence in subsurface waters and subsequently generates



meridional currents from both the northern and southern subtropical gyres toward the equator. These gyres ventilate the upper Equatorial Undercurrent (U-EUC), contributing approximately 9 Sv of the total 28 Sv contribution at 140°W, thus accounting for nearly one third of the upper EUC flow (Grenier et al., 2011).

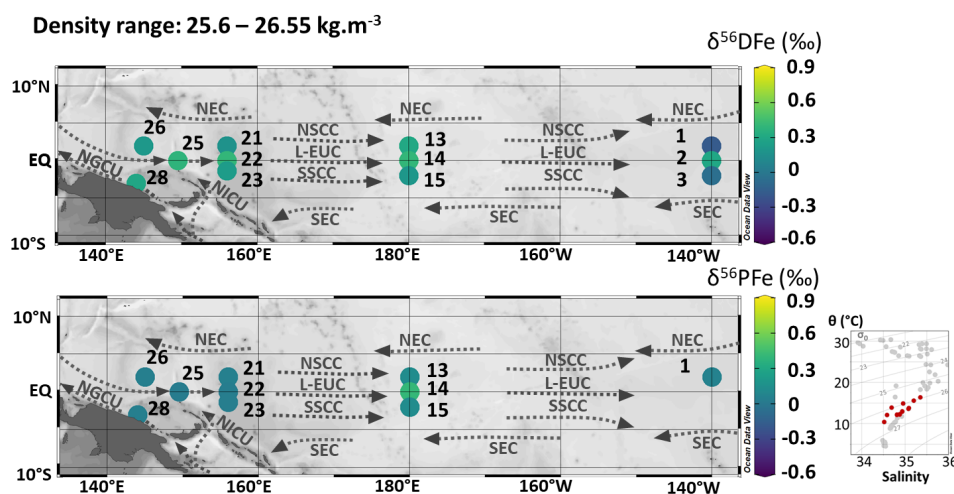
We observed that $\delta^{56}\text{DFe}$ values were equal within uncertainties along the meridional transects between 2°N and 2°S (+0.40 ‰, +0.37 ‰ and +0.28 ‰ at 156°E, 180°E and 140°W, respectively) and similar consistency is observed for $\delta^{56}\text{PFe}$ (-0.03 ‰, +0.18 ‰ and +0.28 ‰ at the three same sections, Figure 9 and Table 2). This isotopic homogeneity is consistent with the prevailing ocean circulation in the subsurface layer. Zonally, a slight decrease of $\delta^{56}\text{DFe}$ values and a slight increase of $\delta^{56}\text{PFe}$ values were observed eastward.

A comparison of DFe isotopic compositions ($\delta^{56}\text{DFe}$) in EUCFe samples with data from the subtropical gyres provides further insight. While no data are available for the north subtropical gyre, this density layer has been documented in the south subtropical gyre along 170°W (GP19 cruise) at 10°S (Station 19) with $\delta^{56}\text{DFe} = +0.64 \pm 0.32$ ‰, and at the equator (Station 21) with $\delta^{56}\text{DFe} = +0.70 \pm 0.35$ ‰ (GEOTRACES Intermediate Data Product Group, 2023). These two datapoints are in good agreement with each other. They could seem significantly different from our data ($\sim 0.37 \pm 0.1$ ‰ at 180°E), however given their uncertainties, they are in reasonable agreement. They do not help explain the slight eastward decrease of the $\delta^{56}\text{DFe}$ along the equator described above.

Overall, despite small variations these observations suggest a relatively wide isotopic homogeneity at subsurface depths (110 - 220 m) likely driven by equatorial upwelling and the subsequent meridional transport of seawater.

580

5.2.3. Lower part of EUC: Central Waters (170 – 320 m; 25.6 – 26.55 kg.m⁻³)



582

Figure 10. Map of dissolved ($\delta^{56}\text{DFe}$) and particulate ($\delta^{56}\text{PFe}$) iron isotopes for samples with potential densities between 25.6 and 26.55 g.m⁻³. Station numbers are displayed next to the colored dots. Main currents are represented: the lower Equatorial Undercurrent (L-EUC), the North and South Subsurface Countercurrents (NSCC and SSCC), the New Guinea Coastal Undercurrent (NGCU) and the New Ireland Coastal Undercurrent (NICU). In the bottom right



588 corner, potential temperature (θ , $^{\circ}\text{C}$) and salinity (S) of EUFe samples. Samples in this density
589 layer are shown in red.

590

591 The density layer between 25.6 and 26.55 kg.m^{-3} is composed of two water masses: the
592 Western South Pacific Central Water (WSPCW) (stations 1, 2, 3, 14, 15, 22, 23, 25, 28) and the
593 North Pacific Central Water (NPCW) (stations 13, 21, 26). WSPCW is characterized by the
594 salinity maximum of central waters while NPCW represents the salinity minimum. The lower
595 part of the EUC (L-EUC) is located in this density layer (Figure 10). This current is of particular
596 importance, since it is the major vector for the Fe transport along the equator from the western
597 to the eastern Pacific. The lower EUC is not significantly influenced by the equatorial upwelling
598 in the western equatorial Pacific, and water mostly originates from the PNG region (Grenier et
599 al., 2011).

600 Along the equator, at stations 25, 22, 14 and 2, samples have similar DFe isotopic
601 composition (around +0.36 ‰), highlighting the lack of significant additional Fe sources in the
602 lower EUC (Tsuchiya et al., 1989; Radic et al., 2011). $\delta^{56}\text{DFe}$ values are equal within
603 uncertainties (Figure 10 and Table 2). This suggests that the $\delta^{56}\text{DFe}$ signature is maintained
604 over long distances within the EUC, a pattern previously reported by Radic et al. (2011) at two
605 stations, and here confirmed as far east as 140°W. In contrast, $\delta^{56}\text{PFe}$ cannot be evaluated at
606 station 2 due to missing PFe data, and values from stations 22 and 14 displayed significantly
607 different values. These findings confirm the central role of the EUC in DFe transport across the
608 Pacific. While earlier studies based on Fe concentrations suggested such transport (Slemons et
609 al., 2012), isotopic data now confirm this conclusion and the fact that dissolved iron isotopic
610 signature may be preserved, in certain circumstances over more than 7,800 km (from station 25
611 to station 2). Long distance preservation of $\delta^{56}\text{DFe}$ signature has been underlined before for
612 deeper layers, notably in the North Pacific and eastern Pacific with Fe transport from
613 sedimentary and hydrothermal sources (Fitzsimmons et al., 2017; John et al., 2018; Sieber et
614 al., 2024).

615 Samples from stations 1 and 3 differ significantly from the other samples. They are
616 characterized by negative dissolved iron isotopic compositions (-0.19 and -0.06 ‰) (Figure 10
617 and Table 2). They are characterized by oxygen concentrations which are notably lower than
618 those typically found in the core of the EUC (43 and 25 $\mu\text{mol.kg}^{-1}$, compared to typical values
619 around 130 $\mu\text{mol.kg}^{-1}$). The currents supplying these stations, SEC and NEC, originate from
620 the east. These three observations support the conclusion that their Fe content originates at least
621 partially from the Californian and/or Peruvian oxygen minimum zones (OMZ). Those have
622 been documented before, with negative or zero $\delta^{56}\text{DFe}$ values in the Californian OMZ (John et
623 al., 2012), and DFe concentrations and isotopic compositions, around 1 nM and -0.5 ‰,
624 observed around 12°S near the Peruvian coast (85 to 80°W) during the GP16 cruise (John et
625 al., 2018). As above this suggests, a $\delta^{56}\text{DFe}$ signature preservation over long distances, of the
626 order of 6,400 km.

627 In this density layer, that of the lower EUC, iron isotopes reveal the presence of two
628 distinct Fe sources in the central Pacific, lithogenic inputs from Papua New Guinea transported
629 within the EUC, and also an additional eastern source from the eastern Pacific oxygen minimum
630 zones.

631



5.2.4. South Antarctic Mode Water and Lower Central Waters (340 – 480 m; 26.55 – 26.9 kg.m⁻³)

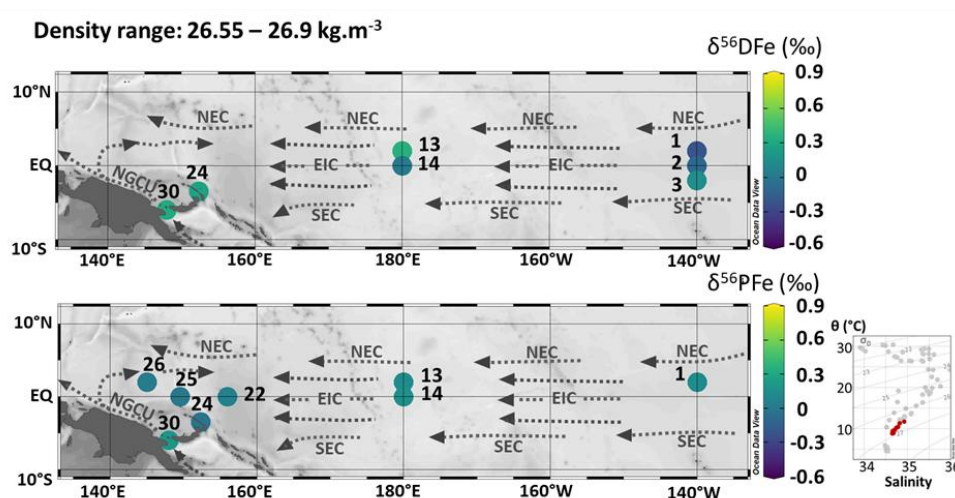


Figure 11. Map of dissolved ($\delta^{56}\text{DFe}$) and particulate ($\delta^{56}\text{PFe}$) iron isotopes for samples with potential densities between 26.55 and 26.9 kg.m⁻³. Station numbers are displayed next to the colored dots. Main currents are represented: the Equatorial Intermediate Current (EIC), the North and South Equatorial Current (NEC and SEC), and the New Guinea Coastal Undercurrent (NGCU). In the bottom right corner, potential temperature (θ , °C) and salinity (S) of EUCFe samples. Samples in this density layer are shown in red.

The density layer between 26.55 and 26.9 kg.m⁻³ is composed of two water masses: the South Antarctic Mode Water (SAMW) (stations 22, 24, 25) and the Western South Pacific Central Water (WSPCW) (stations 1, 2, 3, 13, 14, 26, 30). In contrast to the shallower density layers, where currents predominantly flow eastward, this deeper layer exhibits westward currents (Figures 11).

DFe isotopic compositions at stations 1, 2, 3, 13 and 14 were variable: negative or near zero $\delta^{56}\text{DFe}$ at stations 1, 2 and 14 (between -0.22 and +0.01 ‰) and positive $\delta^{56}\text{DFe}$ at stations 3 and 13 (+0.14 and +0.35 ‰) (Figure 11 and Table 2). $\delta^{56}\text{DFe}$ values increased westward from station 1 (-0.22 ± 0.09 ‰) to station 13 (+0.35 ± 0.07 ‰) and from station 2 (-0.10 ± 0.07 ‰) to station 14 (+0.01 ± 0.07 ‰). This westward increase in $\delta^{56}\text{DFe}$ follows the predominant direction of zonal currents. It is consistent with data from GP19 at 170°W at the equatorial station 21 (-0.07 ± 0.05 ‰, depth of 469 m) (GEOTRACES Intermediate Data Product Group, 2023). In contrast, $\delta^{56}\text{PFe}$ values at stations 1, 13, and 14 were indistinguishable from one another and similar to the UCC reference value. Samples from stations 1, 2, 3, 13 and 14 exhibited low oxygen concentrations (< 64 μmol.kg⁻¹) in contrast to samples from the western equatorial Pacific (stations 22, 24, 25, 26 and 30) where oxygen concentrations ranged from 101 to 162 μmol.kg⁻¹.

These isotopic and oxygen observations suggest an Fe source from the eastern Pacific oxygen minimum zones (OMZ) and a progressive decline in the influence of eastern Pacific waters with the increase of $\delta^{56}\text{DFe}$ westward. It is consistent with our understanding of large-scale circulation patterns at these depths across the Pacific basin, and with the signatures of these areas as described above (John et al., 2012, 2018). In contrast, particulate data were



indistinguishable from those of the UCC all along the EUCCFe cruise and therefore do not reflect hydrodynamic structures.

665

5.2.5. Intermediate Waters (SeqIW and AAIW) (720 – 1,000 m; 27.1 – 27.4 kg.m⁻³)

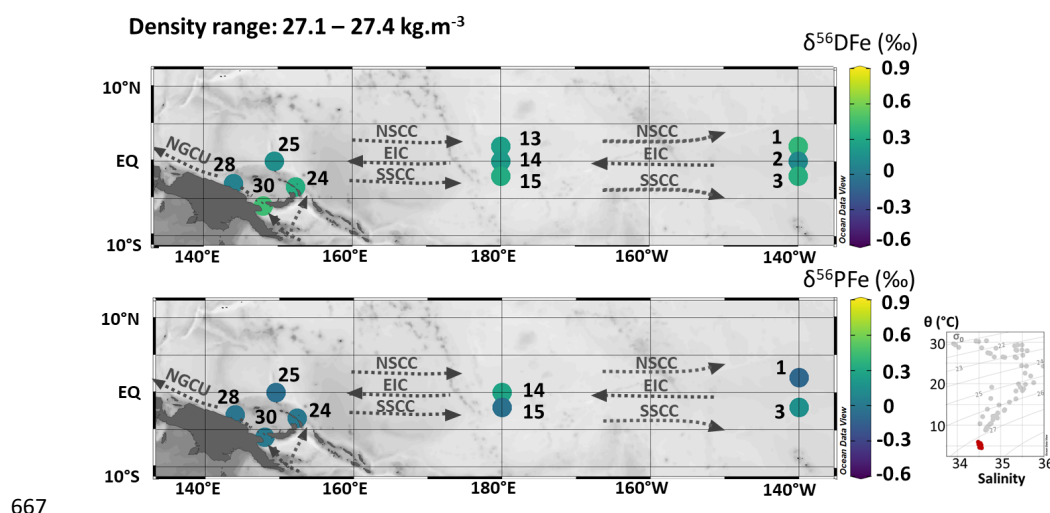


Figure 12. Map of dissolved ($\delta^{56}\text{DFe}$) and particulate ($\delta^{56}\text{PFe}$) iron isotopes for samples with potential densities between 27.1 and 27.4 kg.m⁻³. Station numbers are displayed next to the colored dots. Main currents are represented: the Equatorial Intermediate Current (EIC), the North and South Subsurface Countercurrents (NSCC and SSCC), and the New Guinea Coastal Undercurrent (NGCU). In the bottom right corner, potential temperature (θ , °C) and salinity (S) of EUCFe samples. Samples in this density layer are shown in red.

The density layer between 27.1 and 27.4 kg.m⁻³ is composed of two intermediate water masses: the South Equatorial Intermediate Water (SeqIW) (stations 1, 2, 3, 13, 14, 15, 25) and the Antarctic Intermediate Water (AAIW) (stations 24, 28, 30) (Figure 12). In this layer, the Equatorial Intermediate Current (EIC), a westward current, is surrounded by two eastward currents, the North and South Subsurface Countercurrents (NSCC and SSCC). The water of the EIC is sheared between the NSCC and SSCC currents at about 2°N and 2°S, causing mixing of water brought in by different currents.

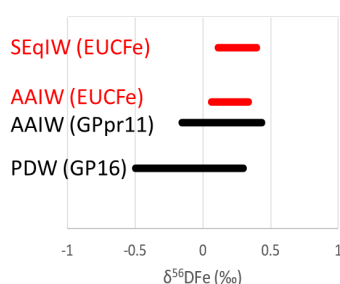
Along the equator, a uniform $\delta^{56}\text{DFe}$ signature was observed between stations 2, 14 and 25, around +0.15 ‰. North and south of it, in the NSCC and the SSCC, the $\delta^{56}\text{DFe}$ signatures were significantly heavier, around +0.32 ‰ and +0.34 ‰ respectively, and did not vary significantly zonally. This is consistent with the hydrodynamic structure (westward flowing EIC at the Equator and eastward flowing NSCC and SSCC at 2°N and 2°S) and may also reflect slightly lighter signatures originating from the eastern Pacific compared to the western Pacific. In contrast, no such consistency was observed for the $\delta^{56}\text{PFe}$ values.

Figure 13 compares $\delta^{56}\text{DFe}$ of the AAIW and SeqIW from this study with data from the South Pacific, GPpr11 (in the Southern Ocean, south of Australia) and GP16 cruises (John et al., 2018; Ellwood et al., 2020). The EUCFe AAIW signature (sampled at the western stations 24, 28 and 30 only) fell within the range of those previously reported, but displayed a smaller variability (from +0.06 to +0.44 ‰, with an average of +0.28 ‰). As explained previously this likely reflects the impact of particle/dissolved reversible exchange and non-reductive



694 dissolution processes which buffer the isotopic signature of this water mass toward about
695 0.3 ‰, in the PNG area.

696 The SEqIW (sampled at stations 1, 2, 3, 13, 14, 15, and 25) results from the mixing
697 between the AAIW and the Pacific Deep Water (PDW). Its signatures fall within the range
698 observed for those waters masses in previous studies, but 1) they fall in the heavy part of those
699 ranges and 2) again have a smaller variability (from +0.11 to +0.40‰, average value of
700 +0.24‰). This confirms 1) the large contribution of AAIW to the iron content of SEqIW and
701 the fact that AAIW transits from the South through the PNG area and notably Vitiaz Strait
702 before spreading in the equatorial band, and 2) that the PDW contributing to the SEqIW reaches
703 the Equatorial band with minor contribution from eastern Pacific OMZ derived iron,
704 characterized by light isotopic signatures (John et al 2018).



705

706 Figure 13. Comparison of $\delta^{56}\text{DFe}$ values in different water masses: the SEqIW sampled during
707 EUCFe cruise (this study), the AAIW sampled during EUCFe (this study) and GPpr11 cruises
708 (Ellwood et al., 2020) and the PDW sampled during GP16 cruise (John et al., 2018).

709

710 6. CONCLUSIONS

711 Figure 14 shows the main conclusions resulting from study of the concentrations and
712 isotope compositions for iron in the upper 1,000 meters of the water column between 140°E
713 and 140°W.

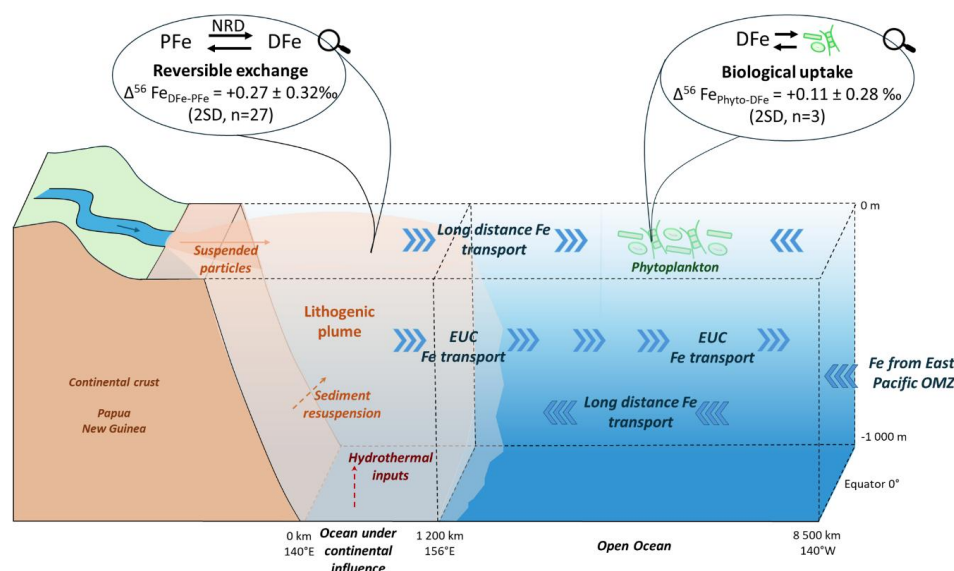


Figure 14. Illustration of Fe transport and transformation along the EUCFe cruise along the equator from the surface to 1,000 meters depth. OMZ stands for oxygen minimum zone.

The goal of the EUCFe cruise was to determine the distribution of Fe along the equator between Papua New Guinea (PNG) and 140°W and to investigate the role of the Equatorial Undercurrent (EUC) in the Fe supply to the central equatorial Pacific. This study reports seawater Fe concentrations and isotopic compositions ($\delta^{56}\text{Fe}$) in both the dissolved (DFe) and particulate (PFe) phases. By adding data from 11 additional stations, this work significantly enriches the data previously published at four stations from the same cruise (Radic et al., 2011; Labatut et al., 2014). The isotopic compositions ranged from -0.25 to +0.79 ‰ for dissolved iron and from -0.56 to +0.48 ‰ for particulate iron. Two distinct groups of stations were identified on the basis of Fe concentrations: western Pacific stations displaying PFe and DFe concentrations approximately seven times and twice larger than typical open ocean concentrations, respectively (stations 21, 22, 23, 24, 25, 26, 28, and 30, all located coast within 1,200 km of the Papua New Guinea coast) and central Pacific open ocean stations, with PFe and DFe typical of the open ocean (stations 1, 2, 3, 7, 13, 14, and 15).

In the western equatorial Pacific, a large predominance of PFe concentrations over that of DFe was observed (80% PFe compared to total Fe, on average). The isotope signature of these particles approaching that of the upper continental crust confirms the major influence of previously documented lithogenic inputs from PNG in this area (Milliman et al., 1999). At two stations, distinctly light $\delta^{56}\text{DFe}$ and $\delta^{56}\text{PFe}$ signatures suggested local hydrothermal inputs. At all stations of this western area, a systematic positive difference between $\delta^{56}\text{DFe}$ and $\delta^{56}\text{PFe}$ was observed, $\Delta^{56}\text{Fe}_{\text{DFe-PFe}} = +0.27 \pm 0.32\text{‰}$ (2SD, n=27). This is interpreted as the result of equilibrium isotopic fractionation resulting from a permanent and reversible exchange between dissolved and particulate Fe phases. This probably reflects processes similar to the reversible scavenging process proposed for Th or REE (Bacon and Anderson, 1982; Nozaki et al., 1987; Nozaki and Alibo, 2003), as previously proposed (Abadie et al., 2017). Isotopic signatures suggest that Fe is primarily released via non-reductive release of dissolved Fe from suspended particles and/or oxic sediment.

In the open ocean, between 180°E and 140°W, data from the chlorophyll maximum layer were used to estimate isotopic fractionation associated with phytoplankton uptake. Our



745 data suggest that isotopic fractionation during phytoplankton uptake is small, on the order of a
746 few tenths of per mil. Just below this layer, within the upper EUC, $\delta^{56}\text{Fe}$ values remain
747 homogeneous across a broad region spanning 2°N to 2°S and 156°E to 140°W , consistent with
748 equatorial upwelling and meridional Fe inputs. In the lower EUC, a DFe isotopic signature of
749 $\sim +0.36\text{‰}$, from the Papua New Guinea area all the way eastward at least to 140°W , confirms
750 the origin of the DFe carried within this current toward the HNCL area. However, an additional
751 Fe source was identified bordering the lower EUC at 2°N and 2°S likely originating from the
752 oxygen minimum zones (OMZ) of the eastern Pacific. This OMZ Fe source is also traced deeper
753 within central waters (200–500 m depth). The preservation of distinct Fe isotopic signatures
754 over long distances, 7,800 km, is a key observation of this study. Finally, the limited variability
755 of the $\delta^{56}\text{DFe}$ signatures in intermediate waters, average of $+0.24\text{‰}$, confirms the major
756 influence of AAIW transiting through the PNG area in the intermediate waters in the EUCFe
757 area.

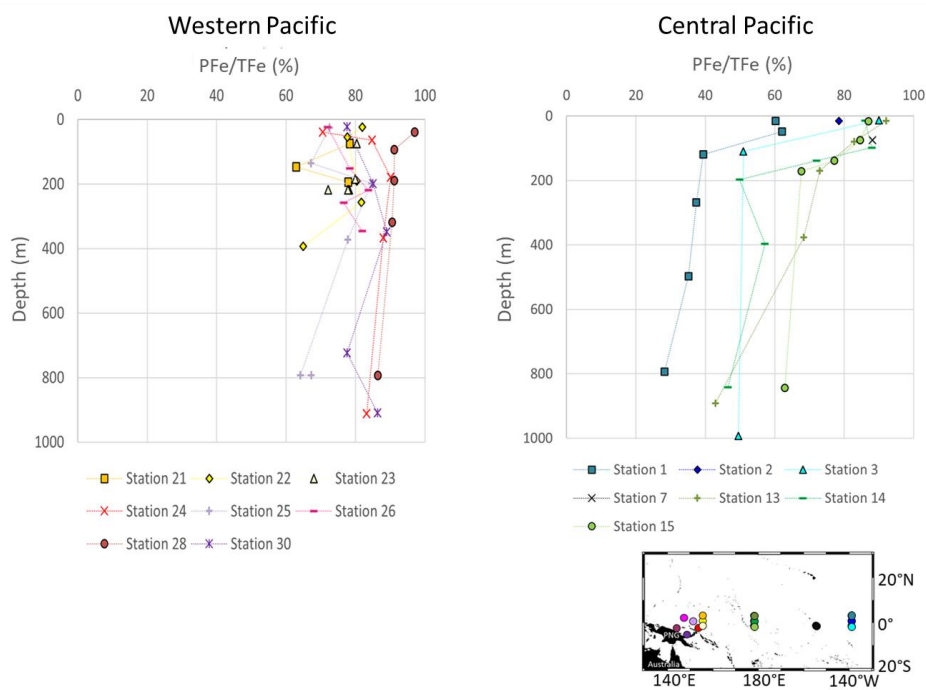
758 In conclusion, this study demonstrates the substantial influence of lithogenic inputs
759 along ocean margins, where the water column (at least down to 1000 m) is affected by
760 permanent and reversible exchange between dissolved and particulate phases. It suggests the
761 significance of non-reductive processes releasing dissolved iron from particulate iron. This non-
762 reductive dissolution (NRD), occurring either at the sediment/seawater interface, i.e., external
763 sources, or within the water column, i.e., internal processes. This highlights the need for a better
764 understanding of these non-reductive DFe – PFe interactions, through in situ explorations,
765 experimental work and biogeochemical modelling. Such processes likely influence the
766 biogeochemical cycling of multiple elements. This study also allowed identification of long-
767 distance iron transport by ocean currents and clarified the key role of the Equatorial
768 Undercurrent (EUC). Finally, it suggests minor fractionation associated to phytoplankton
769 uptake.

770



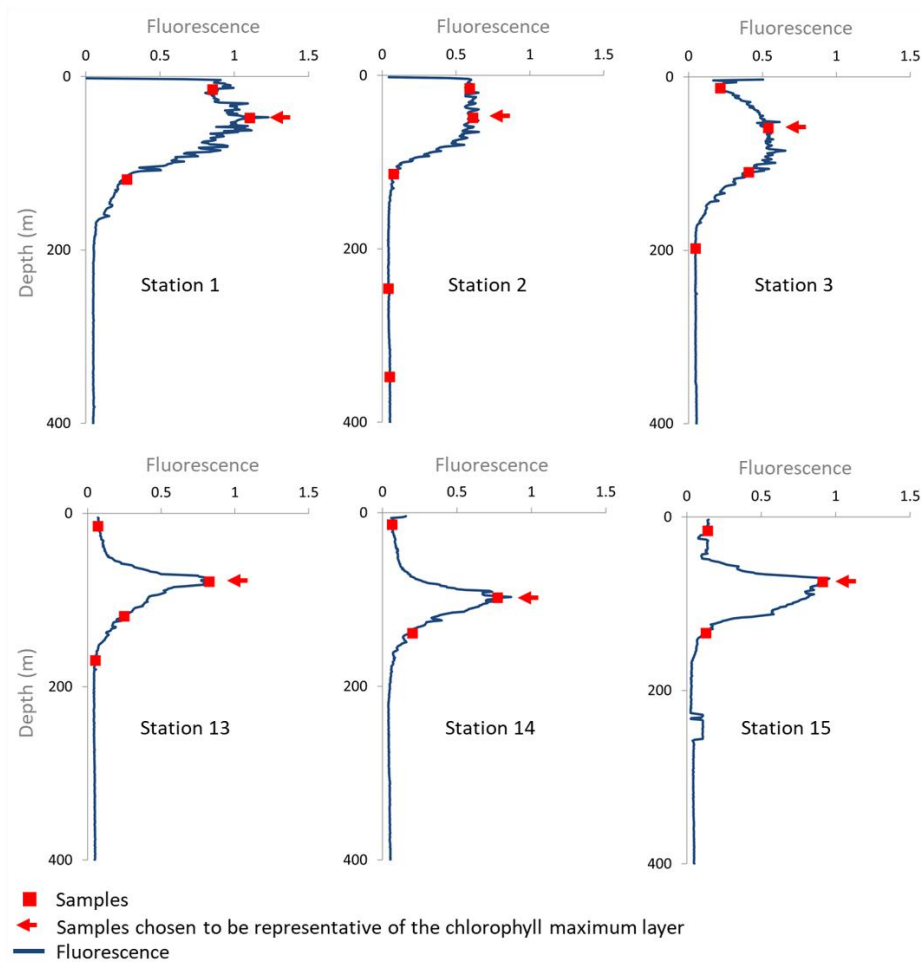
APPENDICE A

Figure A1. Fraction of particulate Fe (PFe) relative to total Fe (TFe) (%) in the western and central equatorial Pacific.





777 **Figure A2.** EUCCFe cruise fluorescence profiles and sampling depth. Note that this fluorescence
778 profiles have been measured in the closest (in time) Niskin rosette cast at the same station.
779 Samples chosen as representative of the chlorophyll maximum are shown by the (←) symbol.



780

781 **Table A1.** Concentrations of particulate Fe and Al, dissolved isotopic composition, estimated
782 fractions of particulate phytoplanktonic and lithogenic Fe, isotopic composition of
783 phytoplanktonic particulate Fe and the isotopic fractionation during biological uptake ($\Delta^{56}\text{Fe}_{\text{Phyto} - \text{DFe}}$) in the chlorophyll maximum layer. Uncertainties are reported as 95% confidence
784 levels. Relative uncertainties for Fe and Al concentrations are 4.3 % (95% confidence level).
785

| Station | Depth (m) | PFe _{total} (nmol.kg ⁻¹) | $\delta^{56}\text{DFe}$ (‰) | PAI (nmol.kg ⁻¹) | PFe _{lithogenic} (%) | PFe _{phyto} (%) | $\delta^{56}\text{PFe}_{\text{phyto}}$ (‰) | $\Delta^{56}\text{Fe}_{\text{Phyto} - \text{DFe}}$ (‰) |
|------------|-----------|---|-----------------------------|------------------------------|-------------------------------|--------------------------|--|--|
| Station 1 | 48 | 0.43 | +0.32 ± 0.07 | 0.53 | 61.7 | 38.3 | +0.54 ± 0.19 | +0.22 ± 0.21 |
| Station 2 | 49 | — | +0.14 ± 0.09 | 6.65 | — | — | — | — |
| Station 3 | 59 | — | +0.31 ± 0.07 | 0.67 | — | — | — | — |
| Station 7 | 75 | 0.55 | — | 0.53 | 49.0 | 51.0 | +0.36 ± 0.14 | — |
| Station 13 | 79 | 0.49 | +0.35 ± 0.07 | 0.15 | 15.2 | 84.8 | +0.30 ± 0.12 | -0.05 ± 0.14 |
| Station 14 | 98 | 0.43 | +0.58 ± 0.07 | 0.39 | 45.2 | 54.8 | +0.73 ± 0.17 | +0.15 ± 0.19 |
| Station 15 | 75 | 0.27 | — | 0.22 | 40.4 | 59.6 | +0.46 ± 0.12 | — |



786

787 **DATA AVAILABILITY**

788 All the data used in this article are reported in Table 2. Fe concentration and isotope data
789 are available in the SEANOE data repository (<https://doi.org/10.17882/107774>, Lacan et al.,
790 2025) and will also be included in the GEOTRACES Data Product.

791

792 **AUTHORS CONTRIBUTIONS**

793 J.W.M. was the principal investigator of the EUCFe cruise. F.L. conceived the iron
794 isotope work. M.L., C.P. and FL analyzed the samples. C.C., F.L. and M.L. wrote the article.
795 All co-authors reviewed the manuscript.

796

797 **COMPETING INTERESTS**

798 The authors declare that they have no conflict of interest.

799

800 **ACKNOWLEDGES**

801 Amandine Radic is very much thanked for having carried out a part of the isotope work.
802 Jérôme Chmeleff, Frédéric Candaudap, and Aurélie Marquet are thanked for their support with
803 the ICP-MS at the *Observatoire Midi-Pyrénées*. Oguz Yigiterhan and Joseph Resing for their
804 help around the Goflo bottles. The captain and the crew of the R/V *Kilo Moana* and especially
805 the marine technicians Gabe Foreman, and Daniel Fitzgerald are acknowledged. Jay Cullen
806 from University of Victoria is thanked for lending the trace-metal rosette. This study was
807 funded by French and USA public funds. The CNRS (French National Center for Scientific
808 Research) and the University of Toulouse (France) are thanked. The EUCFe expedition on the
809 R/V *Kilo Moana* was supported by NSF OCE 0425721 (USA, J. Murray). The Fe isotope
810 project was funded by CNRS-INSU ISOFERIX project (France, F. Lacan).

811

812 **FINANCIAL SUPPORT**

813 This study was funded by French and USA public funds. The CNRS (French National
814 Center for Scientific Research) and the University of Toulouse (France) are thanked. The
815 EUCFe expedition on the R/V *Kilo Moana* was supported by NSF OCE 0425721 (USA). The
816 Fe isotope project was funded par CNRS-INSU ISOFERIX project.

817

818

819 **REFERENCES**

820 Abadie, C., Lacan, F., Radic, A., Pradoux, C., and Poitrasson, F.: Iron isotopes reveal distinct
821 dissolved iron sources and pathways in the intermediate versus deep Southern Ocean, *P Natl A*
822 *Sci USA*, 114, 858–863, <https://doi.org/10.1073/pnas.1603107114>, 2017.

823 Auzende, J.-M., Ishibashi, J.-I., Beaudoin, Y., Charlou, J.-L., Delteil, J., Donval, J.-P., Fouquet,
824 Y., Ildefonse, B., Kimura, H., Nishio, Y., Radford-Knoery, J., and Ruøllan, E.: Extensive



- 825 magmatic and hydrothermal activity documented in Manus Basin, *Eos, Transactions American*
826 *Geophysical Union*, 81, 449–453, <https://doi.org/10.1029/00EO00331>, 2000.
- 827 Bacon, M. P. and Anderson, R. F.: Distribution of thorium isotopes between dissolved and
828 particulate forms in the deep sea, *J Geophys Res-Oceans*, 87, 2045–2056,
829 <https://doi.org/10.1029/JC087iC03p02045>, 1982.
- 830 Bennett, S. A., Rouxel, O., Schmidt, K., Garbe-Schönberg, D., Statham, P. J., and German, C.
831 R.: Iron isotope fractionation in a buoyant hydrothermal plume, 5°S Mid-Atlantic Ridge,
832 *Geochim Cosmochim Acta*, 73, 5619–5634, <https://doi.org/10.1016/j.gca.2009.06.027>, 2009.
- 833 Bergquist, B. A. and Boyle, E. A.: Iron isotopes in the Amazon River system: Weathering and
834 transport signatures, *Earth Planet Sc Lett*, 248, 54–68,
835 <https://doi.org/10.1016/j.epsl.2006.05.004>, 2006.
- 836 Bingham, F. M. and Lukas, R.: The distribution of intermediate water in the western equatorial
837 Pacific during January–February 1986, *Deep-Sea Res Pt I*, 42, 1545–1573,
838 [https://doi.org/10.1016/0967-0637\(95\)00064-D](https://doi.org/10.1016/0967-0637(95)00064-D), 1995.
- 839 Bostock, H. C., Opdyke, B. N., and Williams, M. J. M.: Characterising the intermediate depth
840 waters of the Pacific Ocean using $\delta^{13}\text{C}$ and other geochemical tracers, *Deep-Sea Res Pt I*, 57,
841 847–859, <https://doi.org/10.1016/j.dsr.2010.04.005>, 2010.
- 842 Boyle, E. A., John, S., Abouchami, W., Adkins, J. F., Echegoyen-Sanz, Y., Ellwood, M., Flegal,
843 A. R., Fornace, K., Gallon, C., Galer, S., Gault-Ringold, M., Lacan, F., Radic, A., Rehkamper,
844 M., Rouxel, O., Sohrin, Y., Stirling, C., Thompson, C., Vance, D., Xue, Z., and Zhao, Y.:
845 GEOTRACES IC1 (BATS) contamination-prone trace element isotopes Cd, Fe, Pb, Zn, Cu,
846 and Mo intercalibration, *Limno Oceanogr-Meth*, 10, 653–665,
847 <https://doi.org/10.4319/lom.2012.10.653>, 2012.
- 848 Butt, J. and Lindstrom, E.: Currents off the east coast of New Ireland, Papua New Guinea, and
849 their relevance to regional undercurrents in the western equatorial Pacific Ocean, *J Geophys*
850 *Res-Oceans*, 99, 12503–12514, <https://doi.org/10.1029/94JC00399>, 1994.
- 851 Camin, C., Lacan, F., Pradoux, C., Labatut, M., Johansen, A., and Murray, J. W.: Iron isotopes
852 suggest significant aerosol dissolution over the Pacific Ocean, *Atmos Chem Phys*, 25, 8213–
853 8228, <https://doi.org/10.5194/acp-25-8213-2025>, 2025.
- 854 Cardinal, D., Dehairs, F., Cattaldo, T., and André, L.: Geochemistry of suspended particles in
855 the Subantarctic and Polar Frontal zones south of Australia: Constraints on export and advection
856 processes, *J Geophys Res-Oceans*, 106, 31637–31656, <https://doi.org/10.1029/2000JC000251>,
857 2001.
- 858 Ccanccapa-Cartagena, A., Chavez-Gonzales, F. D., Paredes, B., Vera, C., Gutierrez, G.,
859 Valencia, R., Lucia Paz Alcázar, A., Zyaykina, N. N., Filley, T. R., and Jafvert, C. T.: Seasonal
860 differences in trace metal concentrations in the major rivers of the hyper-arid southwestern
861 Andes basins of Peru, *J Environ Manage*, 344, 118493,
862 <https://doi.org/10.1016/j.jenvman.2023.118493>, 2023.
- 863 Chisholm, S. W. and Morel, F. M. M.: What controls phytoplankton production in nutrient-rich
864 areas of the open sea?, in: *Limnology and Oceanography*, American Society of Limnology and
865 *Oceanography Symposium*, San-Marcos, California, U1507–U1511, 1991.
- 866 Coale, K. H., Fitzwater, S. E., Gordon, R. M., Johnson, K. S., and Barber, R. T.: Control of
867 community growth and export production by upwelled iron in the equatorial Pacific Ocean,
868 *Nature*, 379, 621–624, <https://doi.org/10.1038/379621a0>, 1996.



- 869 Cohen, N. R., Noble, A. E., Moran, D. M., McIlvin, M. R., Goepfert, T. J., Hawco, N. J.,
870 German, C. R., Horner, T. J., Lamborg, C. H., McCrow, J. P., Allen, A. E., and Saito, M. A.:
871 Hydrothermal trace metal release and microbial metabolism in the northeastern Lau Basin of
872 the South Pacific Ocean, *Biogeosciences*, 18, 5397–5422, [https://doi.org/10.5194/bg-18-5397-](https://doi.org/10.5194/bg-18-5397-2021)
873 2021, 2021.
- 874 Conway, T. M. and John, S. G.: Quantification of dissolved iron sources to the North Atlantic
875 Ocean, *Nature*, 511, 212–215, <https://doi.org/10.1038/nature13482>, 2014.
- 876 Conway, T. M., John, S. G., and Lacan, F.: Intercomparison of dissolved iron isotope profiles
877 from reoccupation of three GEOTRACES stations in the Atlantic Ocean, *Mar Chem*, 183, 50–
878 61, <https://doi.org/10.1016/j.marchem.2016.04.007>, 2016.
- 879 Cravatte, S., Kestenare, E., Marin, F., Dutrieux, P., and Firing, E.: Subthermocline and
880 Intermediate Zonal Currents in the Tropical Pacific Ocean: Paths and Vertical Structure, *J Phys*
881 *Oceanogr*, 47, 2305–2324, <https://doi.org/10.1175/JPO-D-17-0043.1>, 2017.
- 882 Criss, R. E.: *Principles of Stable Isotope Distribution*, Oxford University Press, Oxford, New
883 York, 264 pp., ISBN 978-0-19-756119-5, 1999.
- 884 Dammschäuser, A.: Distribution and behavior of the lithogenic tracers aluminium and titanium
885 in the upper water column of the Atlantic Ocean, Faculty of Mathematics and Natural Sciences
886 Christian-Albrechts-Universität zu Kiel, [https://nbn-resolving.org/urn:nbn:de:gbv:8-diss-](https://nbn-resolving.org/urn:nbn:de:gbv:8-diss-81211)
887 81211 (last access:16 November 2024), 2012.
- 888 Ellwood, M. J., Hutchins, D. A., Lohan, M. C., Milne, A., Nasemann, P., Nodder, S. D., Sander,
889 S. G., Strzepek, R., Wilhelm, S. W., and Boyd, P. W.: Iron stable isotopes track pelagic iron
890 cycling during a subtropical phytoplankton bloom, *P Natl Acad Sci USA*, 112, E15–E20,
891 <https://doi.org/10.1073/pnas.1421576112>, 2015.
- 892 Ellwood, M. J., Strzepek, R. F., Strutton, P. G., Trull, T. W., Fourquez, M., and Boyd, P. W.:
893 Distinct iron cycling in a Southern Ocean eddy, *Nat Commun*, 11, 825,
894 <https://doi.org/10.1038/s41467-020-14464-0>, 2020.
- 895 Emery, W. J. and Meincke, J.: Global water masses : summary and review, *Oceanol Acta*, 9,
896 383–391, ISSN 0399-1784, 1986.
- 897 Fantle, M. S. and DePaolo, D. J.: Iron isotopic fractionation during continental weathering,
898 *Earth Planet Sc Lett*, 228, 547–562, <https://doi.org/10.1016/j.epsl.2004.10.013>, 2004.
- 899 Fiedler, P. C. and Talley, L. D.: Hydrography of the eastern tropical Pacific: A review, *Prog*
900 *Oceanogr*, 69, 143–180, <https://doi.org/10.1016/j.pocean.2006.03.008>, 2006.
- 901 Fine, R. A., Lukas, R., Bingham, F. M., Warner, M. J., and Gammon, R. H.: The western
902 equatorial Pacific: A water mass crossroads, *Journal of Geophysical Research: Oceans*, 99,
903 25063–25080, <https://doi.org/10.1029/94JC02277>, 1994.
- 904 Fitzsimmons, J. N., John, S. G., Marsay, C. M., Hoffman, C. L., Nicholas, S. L., Toner, B. M.,
905 German, C. R., and Sherrell, R. M.: Iron persistence in a distal hydrothermal plume supported
906 by dissolved–particulate exchange, *Nature Geosci*, 10, 195–201,
907 <https://doi.org/10.1038/ngeo2900>, 2017.
- 908 Flament, P., Mattielli, N., Aimo, L., Choël, M., Deboudt, K., Jong, J. de, Rimetz-Planchon, J.,
909 and Weis, D.: Iron isotopic fractionation in industrial emissions and urban aerosols,
910 *Chemosphere*, 73, 1793–1798, <https://doi.org/10.1016/j.chemosphere.2008.08.042>, 2008.



- 911 Frank, M., Eisenhauer, A., Bonn, W. J., Walter, P., Grobe, H., Kubik, P. W., Ditttrich-Hannen,
912 B., and Mangini, A.: Sediment redistribution versus paleoproductivity change: Weddell Sea
913 margin sediment stratigraphy and biogenic particle flux of the last 250,000 years deduced from
914 230Thex, 10Be and biogenic barium profiles, *Earth Planet Sc Lett*, 136, 559–573,
915 [https://doi.org/10.1016/0012-821X\(95\)00161-5](https://doi.org/10.1016/0012-821X(95)00161-5), 1995.
- 916 GEOTRACES Intermediate Data Product Group: The GEOTRACES Intermediate Data
917 Product 2021v2 (IDP2021v2) (2), [https://doi.org/10.5285/ff46f034-f47c-05f9-e053-](https://doi.org/10.5285/ff46f034-f47c-05f9-e053-6c86abc0dc7e)
918 6c86abc0dc7e, [data set], 2023.
- 919 Germineaud, C., Ganachaud, A., Sprintall, J., Cravatte, S., Eldin, G., Albery, M. S., and Privat,
920 E.: Pathways and Water Mass Properties of the Thermocline and Intermediate Waters in the
921 Solomon Sea, *J Phys Oceanogr*, 46, 3031–3049, <https://doi.org/10.1175/JPO-D-16-0107.1>,
922 2016.
- 923 Gordon, R. M., Coale, K. H., and Johnson, K. S.: Iron distributions in the equatorial Pacific:
924 Implications for new production, *Limnol Oceanogr*, 42, 419–431,
925 <https://doi.org/10.4319/lo.1997.42.3.0419>, 1997.
- 926 Grenier, M.: Le rôle du pacifique tropical sud-ouest dans la fertilisation du pacifique équatorial :
927 couplage dynamique et multi-traceur, *These de doctorat*, Toulouse 3, 205 pp.,
928 <https://theses.hal.science/tel-00876092> (last access: 4 April 2024), 2012.
- 929 Grenier, M., Cravatte, S., Blanke, B., Menkes, C., Koch-Larrouy, A., Durand, F., Melet, A.,
930 and Jeandel, C.: From the western boundary currents to the Pacific Equatorial Undercurrent:
931 Modeled pathways and water mass evolutions, *Journal of Geophysical Research: Oceans*, 116,
932 <https://doi.org/10.1029/2011JC007477>, 2011.
- 933 Grenier, M., Jeandel, C., Lacan, F., Vance, D., Venchiarutti, C., Cros, A., and Cravatte, S.:
934 From the subtropics to the central equatorial Pacific Ocean: Neodymium isotopic composition
935 and rare earth element concentration variations, *J Geophys Res-Oceans*, 118, 592–618,
936 <https://doi.org/10.1029/2012JC008239>, 2013.
- 937 Hayes, J.: *An Introduction to Isotopic Calculations*, Woods Hole Oceanographic Institution,
938 <https://doi.org/10.1575/1912/27058>, 2004.
- 939 Homoky, W. B., Severmann, S., Mills, R. A., Statham, P. J., and Fones, G. R.: Pore-fluid Fe
940 isotopes reflect the extent of benthic Fe redox recycling: Evidence from continental shelf and
941 deep-sea sediments, *Geology*, 37, 751–754, <https://doi.org/10.1130/G25731A.1>, 2009.
- 942 Homoky, W. B., Conway, T. M., John, S. G., König, D., Deng, F., Tagliabue, A., and Mills, R.
943 A.: Iron colloids dominate sedimentary supply to the ocean interior, *P Natl Acad Sci USA*, 118,
944 e2016078118, <https://doi.org/10.1073/pnas.2016078118>, 2021.
- 945 Ingri, J., Malinovsky, D., Rodushkin, I., Baxter, D. C., Widerlund, A., Andersson, P.,
946 Gustafsson, Ö., Forsling, W., and Öhlander, B.: Iron isotope fractionation in river colloidal
947 matter, *Earth Planet Sc Lett*, 245, 792–798, <https://doi.org/10.1016/j.epsl.2006.03.031>, 2006.
- 948 John, S. G., Mendez, J., Moffett, J., and Adkins, J.: The flux of iron and iron isotopes from San
949 Pedro Basin sediments, *Geochim Cosmochim Ac*, 93, 14–29,
950 <https://doi.org/10.1016/j.gca.2012.06.003>, 2012.
- 951 John, S. G., Helgoe, J., Townsend, E., Weber, T., DeVries, T., Tagliabue, A., Moore, K., Lam,
952 P., Marsay, C. M., and Till, C.: Biogeochemical cycling of Fe and Fe stable isotopes in the
953 Eastern Tropical South Pacific, *Mar Chem*, 201, 66–76,
954 <https://doi.org/10.1016/j.marchem.2017.06.003>, 2018.



- 955 Kaupp, L. J., Measures, C. I., Selph, K. E., and Mackenzie, F. T.: The distribution of dissolved
956 Fe and Al in the upper waters of the Eastern Equatorial Pacific, *Deep-Sea Res Pt II*, 58, 296–
957 310, <https://doi.org/10.1016/j.dsr2.2010.08.009>, 2011.
- 958 Kineke, G. C., Woolfe, K. J., Kuehl, S. A., Milliman, J. D., Dellapenna, T. M., and Purdon, R.
959 G.: Sediment export from the Sepik River, Papua New Guinea: evidence for a divergent
960 sediment plume, *Cont Shelf Res*, 20, 2239–2266, [https://doi.org/10.1016/S0278-](https://doi.org/10.1016/S0278-4343(00)00069-8)
961 4343(00)00069-8, 2000.
- 962 Klar, J. K., Schlosser, C., Milton, J. A., Woodward, E. M. S., Lacan, F., Parkinson, I. J.,
963 Achterberg, E. P., and James, R. H.: Sources of dissolved iron to oxygen minimum zone waters
964 on the Senegalese continental margin in the tropical North Atlantic Ocean: Insights from iron
965 isotopes, *Geochim Cosmochim Acta*, 236, 60–78, <https://doi.org/10.1016/j.gca.2018.02.031>,
966 2018.
- 967 Kuehl, S. A., Brunskill, G. J., Burns, K., Fugate, D., Kniskern, T., and Meneghini, L.: Nature
968 of sediment dispersal off the Sepik River, Papua New Guinea: preliminary sediment budget and
969 implications for margin processes, *Cont Shelf Res*, 24, 2417–2429,
970 <https://doi.org/10.1016/j.csr.2004.07.016>, 2004.
- 971 Kurisu, M., Sakata, K., Miyamoto, C., Takaku, Y., Iizuka, T., and Takahashi, Y.: Variation of
972 Iron Isotope Ratios in Anthropogenic Materials Emitted through Combustion Processes, *Chem*
973 *Lett*, 45, 970–972, <https://doi.org/10.1246/cl.160451>, 2016.
- 974 Labatut, M., Lacan, F., Pradoux, C., Chmeleff, J., Radic, A., Murray, J. W., Poitrasson, F.,
975 Johansen, A. M., and Thil, F.: Iron sources and dissolved-particulate interactions in the seawater
976 of the Western Equatorial Pacific, iron isotope perspectives, *Global Biogeochem Cy*, 28, 1044–
977 1065, <https://doi.org/10.1002/2014GB004928>, 2014.
- 978 Lacan, F. and Jeandel, C.: Tracing Papua New Guinea imprint on the central Equatorial Pacific
979 Ocean using neodymium isotopic compositions and Rare Earth Element patterns, *Earth Planet*
980 *Sc Lett*, 186, 497–512, [https://doi.org/10.1016/S0012-821X\(01\)00263-1](https://doi.org/10.1016/S0012-821X(01)00263-1), 2001.
- 981 Lacan, F., Radic, A., Jeandel, C., Poitrasson, F., Sarthou, G., Pradoux, C., and Freydier, R.:
982 Measurement of the isotopic composition of dissolved iron in the open ocean, *Geophys Res*
983 *Lett*, 35, L24610, <https://doi.org/10.1029/2008GL035841>, 2008.
- 984 Lacan, F., Radic, A., Labatut, M., Jeandel, C., Poitrasson, F., Sarthou, G., Pradoux, C.,
985 Chmeleff, J., and Freydier, R.: High-Precision Determination of the Isotopic Composition of
986 Dissolved Iron in Iron Depleted Seawater by Double Spike Multicollector-ICPMS, *Anal Chem*,
987 82, 7103–7111, <https://doi.org/10.1021/ac1002504>, 2010.
- 988 Lacan, F., Artigue, L., Klar, J. K., Pradoux, C., Chmeleff, J., and Freydier, R.: Interferences
989 and Matrix Effects on Iron Isotopic Composition Measurements by ^{57}Fe - ^{58}Fe Double-Spike
990 Multi-Collector Inductively Coupled Plasma Mass Spectrometry; the Importance of Calcium
991 and Aluminum Interferences, *Front Environ Chem*, 2,
992 <https://doi.org/10.3389/fenvc.2021.692025>, 2021.
- 993 Lacan, F., Pradoux, C., Dutrieux, P., Murray, J. W., Johansen, A., Radic, A., and Labatut, M.:
994 CTD, dissolved oxygen concentrations, iron concentrations and isotopic compositions in the
995 filtered seawater, seawater suspended particles and aerosols, during the EUFe cruise,
996 KM0625, in the Equatorial Pacific Ocean, SEANOE [data set],
997 <https://doi.org/10.17882/107774>, 2025.



- 998 Mackey, D. J., O’Sullivan, J. E. Os., and Watson, R. J.: Iron in the western Pacific: a riverine
999 or hydrothermal source for iron in the Equatorial Undercurrent?, *Deep-Sea Res Pt I*, 49, 877–
1000 893, [https://doi.org/10.1016/S0967-0637\(01\)00075-9](https://doi.org/10.1016/S0967-0637(01)00075-9), 2002.
- 1001 Marsay, C. M., Lam, P. J., Heller, M. I., Lee, J.-M., and John, S. G.: Distribution and isotopic
1002 signature of ligand-leachable particulate iron along the GEOTRACES GP16 East Pacific Zonal
1003 Transect, *Mar Chem*, 201, 198–211, <https://doi.org/10.1016/j.marchem.2017.07.003>, 2018.
- 1004 Martin, J. H.: Iron as a Limiting Factor in Oceanic Productivity, in: *Primary Productivity and*
1005 *Biogeochemical Cycles in the Sea*, edited by: Falkowski, P. G., Woodhead, A. D., and Vivirito,
1006 K., Springer, Boston, MA, 123–137, https://doi.org/10.1007/978-1-4899-0762-2_8, 1992.
- 1007 McCartney, M. S.: Subantarctic Mode Water, Woods Hole Oceanographic Institution
1008 Contribution 3773, 103–119,
1009 <https://www.whoi.edu/science/PO/people/mmccartney/pdfs/McCartney77.pdf> (last access: 15
1010 January 2025), 1977.
- 1011 McManus, J., Berelson, W. M., Hammond, D. E., and Klinkhammer, G. P.: Barium Cycling in
1012 the North Pacific: Implications for the Utility of Ba as a Paleoproductivity and Paleoalkalinity
1013 Proxy, *Paleoceanography*, 14, 53–61, <https://doi.org/10.1029/1998PA900007>, 1999.
- 1014 Milliman, J. D.: Sediment discharge to the ocean from small mountainous rivers: The New
1015 Guinea example, *Geo-Mar Lett*, 15, 127–133, <https://doi.org/10.1007/BF01204453>, 1995.
- 1016 Milliman, J. D. and Syvitski, J. P. M.: Geomorphic/Tectonic Control of Sediment Discharge to
1017 the Ocean: The Importance of Small Mountainous Rivers, *The Journal of Geology*, 100, 525–
1018 544, <https://doi.org/10.1086/629606>, 1992.
- 1019 Milliman, J. D., Farnsworth, K. L., and Albertin, C. S.: Flux and fate of fluvial sediments
1020 leaving large islands in the East Indies, *J Sea Res*, 41, 97–107, [https://doi.org/10.1016/S1385-1101\(98\)00040-9](https://doi.org/10.1016/S1385-1101(98)00040-9), 1999.
- 1022 Morel, F. M. M., Lam, P. J., and Saito, M. A.: Trace Metal Substitution in Marine
1023 Phytoplankton, *Annu Rev Earth Pl Sc*, 48, 491–517, <https://doi.org/10.1146/annurev-earth-053018-060108>, 2020.
- 1025 Murray, J. W., Barber, R. T., Roman, M. R., Bacon, M. P., and Feely, R. A.: Physical and
1026 Biological Controls on Carbon Cycling in the Equatorial Pacific, *Science*, 266, 58–65,
1027 <https://doi.org/10.1126/science.266.5182.58>, 1994.
- 1028 Murray, R. W., Leinen, M., and Isern, A. R.: Biogenic flux of Al to sediment in the central
1029 equatorial Pacific Ocean: Evidence for increased productivity during glacial periods,
1030 *Paleoceanography*, 8, 651–670, <https://doi.org/10.1029/93PA02195>, 1993.
- 1031 Nozaki, Y. and Alibo, D. S.: Dissolved rare earth elements in the Southern Ocean, southwest
1032 of Australia: Unique patterns compared to the South Atlantic data, *Geochem J*, 37, 47–62,
1033 <https://doi.org/10.2343/geochemj.37.47>, 2003.
- 1034 Nozaki, Y., Yang, H.-S., and Yamada, M.: Scavenging of thorium in the ocean, *J Geophys Res-*
1035 *Oceans*, 92, 772–778, <https://doi.org/10.1029/JC092iC01p00772>, 1987.
- 1036 Philander, S. G. H.: equatorial undercurrent: Measurements and theories, *Rev Geophys*, 11,
1037 513–570, <https://doi.org/10.1029/RG011i003p00513>, 1973.
- 1038 Pickard, G. L. and Emery, W. J.: *Descriptive Physical Oceanography*, Elsevier, 348 pp., ISBN
1039 978-0-7506-2759-7, 1990.



- 1040 Poitrasson, F.: On the iron isotope homogeneity level of the continental crust, *Chem Geol*, 235,
1041 195–200, <https://doi.org/10.1016/j.chemgeo.2006.06.010>, 2006.
- 1042 Pollard, R. T., Griffiths, M. J., Cunningham, S. A., Read, J. F., Pérez, F. F., and Ríos, A. F.:
1043 Vivaldi 1991 - A study of the formation, circulation and ventilation of Eastern North Atlantic
1044 Central Water, *Prog Oceanogr*, [https://doi.org/10.1016/S0079-6611\(96\)00008-0](https://doi.org/10.1016/S0079-6611(96)00008-0), 1996.
- 1045 Qu, T. and Lindstrom, E. J.: A Climatological Interpretation of the Circulation in the Western
1046 South Pacific, *J Phys Oceanogr*, 32, 2492–2508, [https://doi.org/10.1175/1520-0485\(2002\)032<2492:ACIOTC>2.0.CO;2](https://doi.org/10.1175/1520-0485(2002)032<2492:ACIOTC>2.0.CO;2), 2002.
- 1048 Qu, T. and Lindstrom, E. J.: Northward Intrusion of Antarctic Intermediate Water in the
1049 Western Pacific, *J Phys Oceanogr*, 34, 2104–2118, [https://doi.org/10.1175/1520-0485\(2004\)034<2104:NIOAIW>2.0.CO;2](https://doi.org/10.1175/1520-0485(2004)034<2104:NIOAIW>2.0.CO;2), 2004.
- 1051 Qu, T., Gao, S., Fukumori, I., Fine, R. A., and Lindstrom, E. J.: Origin and Pathway of
1052 Equatorial 13°C Water in the Pacific Identified by a Simulated Passive Tracer and Its Adjoint,
1053 *J Phys Oceanogr*, 39, 1836–1853, <https://doi.org/10.1175/2009JPO4045.1>, 2009.
- 1054 Radic, A., Lacan, F., and Murray, J. W.: Iron isotopes in the seawater of the equatorial Pacific
1055 Ocean: New constraints for the oceanic iron cycle, *Earth Planet Sc Lett*, 306, 1–10,
1056 <https://doi.org/10.1016/j.epsl.2011.03.015>, 2011.
- 1057 Renagi, O., Ridd, P., and Stieglitz, T.: Quantifying the suspended sediment discharge to the
1058 ocean from the Markham River, Papua New Guinea, *Cont Shelf Res*, 30, 1030–1041,
1059 <https://doi.org/10.1016/j.csr.2010.01.015>, 2010.
- 1060 Resing, J. A., Sedwick, P. N., German, C. R., Jenkins, W. J., Moffett, J. W., Sohst, B. M., and
1061 Tagliabue, A.: Basin-scale transport of hydrothermal dissolved metals across the South Pacific
1062 Ocean, *Nature*, 523, 200–203, <https://doi.org/10.1038/nature14577>, 2015.
- 1063 Rodgers, K. B., Blanke, B., Madec, G., Aumont, O., Ciais, P., and Dutay, J.-C.: Extratropical
1064 sources of Equatorial Pacific upwelling in an OGCM, *Geophys Res Lett*, 30,
1065 <https://doi.org/10.1029/2002GL016003>, 2003.
- 1066 Rouxel, O., Shanks, W. C., Bach, W., and Edwards, K. J.: Integrated Fe- and S-isotope study
1067 of seafloor hydrothermal vents at East Pacific Rise 9–10°N, *Chemical Geology*, 252, 214–227,
1068 <https://doi.org/10.1016/j.chemgeo.2008.03.009>, 2008.
- 1069 Rudnick, R. L. and Gao, S.: 4.1 - Composition of the Continental Crust, in: *Treatise on*
1070 *Geochemistry* (Second Edition), edited by: Holland, H. D. and Turekian, K. K., Elsevier,
1071 Oxford, 1–51, <https://doi.org/10.1016/B978-0-08-095975-7.00301-6>, 2014.
- 1072 Ryan, J. P., Ueki, I., Chao, Y., Zhang, H., Polito, P. S., and Chavez, F. P.: Western Pacific
1073 modulation of large phytoplankton blooms in the central and eastern equatorial Pacific, *Journal*
1074 *of Geophysical Research: Biogeosciences*, 111, <https://doi.org/10.1029/2005JG000084>, 2006.
- 1075 Severmann, S., Johnson, C. M., Beard, B. L., German, C. R., Edmonds, H. N., Chiba, H., and
1076 Green, D. R. H.: The effect of plume processes on the Fe isotope composition of hydrothermally
1077 derived Fe in the deep ocean as inferred from the Rainbow vent site, Mid-Atlantic Ridge,
1078 36°14'N, *Earth Planet Sc Lett*, 225, 63–76, <https://doi.org/10.1016/j.epsl.2004.06.001>, 2004.
- 1079 Severmann, S., Johnson, C. M., Beard, B. L., and McManus, J.: The effect of early diagenesis
1080 on the Fe isotope compositions of porewaters and authigenic minerals in continental margin
1081 sediments, *Geochim Cosmochim Acta*, 70, 2006–2022,
1082 <https://doi.org/10.1016/j.gca.2006.01.007>, 2006.



- 1083 Sharma, M., Polizzotto, M., and Anbar, A. D.: Iron isotopes in hot springs along the Juan de
1084 Fuca Ridge, *Earth Planet Sc Lett*, 194, 39–51, [https://doi.org/10.1016/S0012-821X\(01\)00538-](https://doi.org/10.1016/S0012-821X(01)00538-6)
1085 6, 2001.
- 1086 Shelley, R. U., Roca-Martí, M., Castrillejo, M., Sanial, V., Masqué, P., Landing, W. M., van
1087 Beek, P., Planquette, H., and Sarthou, G.: Quantification of trace element atmospheric
1088 deposition fluxes to the Atlantic Ocean (>40°N; GEOVIDE, GEOTRACES GA01) during
1089 spring 2014, *Deep-Sea Res Pt I*, 119, 34–49, <https://doi.org/10.1016/j.dsr.2016.11.010>, 2017.
- 1090 Sieber, M., Conway, T. M., de Souza, G. F., Hassler, C. S., Ellwood, M. J., and Vance, D.:
1091 Isotopic fingerprinting of biogeochemical processes and iron sources in the iron-limited surface
1092 Southern Ocean, *Earth Planet Sc Lett*, 567, 116967, <https://doi.org/10.1016/j.epsl.2021.116967>,
1093 2021.
- 1094 Sieber, M., Lanning, N. T., Steffen, J. M., Bian, X., Yang, S.-C., Lee, J. M., Weiss, G., Hunt,
1095 H. R., Charette, M. A., Moore, W. S., Hautala, S. L., Hatta, M., Lam, P. J., John, S. G.,
1096 Fitzsimmons, J. N., and Conway, T. M.: Long Distance Transport of Subsurface Sediment-
1097 Derived Iron From Asian to Alaskan Margins in the North Pacific Ocean, *Geophys Res Lett*,
1098 51, e2024GL110836, <https://doi.org/10.1029/2024GL110836>, 2024.
- 1099 Slemons, L., Gorgues, T., Aumont, O., Menkes, C., and Murray, J. W.: Biogeochemical impact
1100 of a model western iron source in the Pacific Equatorial Undercurrent, *Deep Sea Research Part*
1101 *I: Oceanographic Research Papers*, 56, 2115–2128, <https://doi.org/10.1016/j.dsr.2009.08.005>,
1102 2009.
- 1103 Slemons, L., Murray, J. W., Resing, J., Paul, B., and Dutrieux, P.: Western Pacific coastal
1104 sources of iron, manganese, and aluminum to the Equatorial Undercurrent, *Global Biogeochem*
1105 *Cy*, 24, <https://doi.org/10.1029/2009GB003693>, 2010.
- 1106 Slemons, L., Paul, B., Resing, J., and Murray, J. W.: Particulate iron, aluminum, and manganese
1107 in the Pacific equatorial undercurrent and low latitude western boundary current sources, *Mar*
1108 *Chem*, 142–144, 54–67, <https://doi.org/10.1016/j.marchem.2012.08.003>, 2012.
- 1109 Sokolov, S. and Rintoul, S.: Circulation and water masses of the southwest Pacific: WOCE
1110 Section P11, Papua New Guinea to Tasmania, *J Mar Res*, 58, 2000.
- 1111 Stramma, L. and England, M. H.: On the water masses and mean circulation of the South
1112 Atlantic Ocean, *J Geophys Res-Oceans*, 104, 20863–20883,
1113 <https://doi.org/10.1029/1999JC900139>, 1999.
- 1114 Talley, L. D.: Some aspects of ocean heat transport by the shallow, intermediate and deep
1115 overturning circulations, *Geoph Monog Series*, 112, 1–22,
1116 <https://doi.org/10.1029/GM112p0001>, 1999.
- 1117 Talley, L. D.: Freshwater transport estimates and the global overturning circulation: Shallow,
1118 deep and throughflow components, *Prog Oceanogr*, 78, 257–303,
1119 <https://doi.org/10.1016/j.pocean.2008.05.001>, 2008.
- 1120 Talley, L. D., Pickard, G. L., Emery, W. J., and Swift, J. H.: Descriptive Physical
1121 Oceanography: An Introduction, Academic Press, 555 pp., ISBN 978-0-7506-4552-2, 2011.
- 1122 Tian, H.-A., van Manen, M., Bunnell, Z. B., Jung, J., Lee, S. H., Kim, T.-W., Reichert, G.-J.,
1123 Conway, T. M., and Middag, R.: Biogeochemistry of iron in coastal Antarctica: isotopic
1124 insights for external sources and biological uptake in the Amundsen Sea polynyas, *Geochim*
1125 *Cosmochim Ac*, 363, 51–67, <https://doi.org/10.1016/j.gca.2023.10.029>, 2023.



- 1126 Tiangang, W., Kumul, C., Yuhao, Z., Mosusu, N., Bimin, Z., Pei, N., and De Vivo, B.: National-
1127 scale Geochemical Baseline of 69 elements in Papua New Guinea stream sediments, *J Geochem*
1128 *Explor*, 256, 107355, <https://doi.org/10.1016/j.gexplo.2023.107355>, 2024.
- 1129 Tilliette, C., Taillandier, V., Bouruet-Aubertot, P., Grima, N., Maes, C., Montanes, M., Sarthou,
1130 G., Vorrath, M.-E., Arnone, V., Bressac, M., González-Santana, D., Gazeau, F., and Guieu, C.:
1131 Dissolved Iron Patterns Impacted by Shallow Hydrothermal Sources Along a Transect Through
1132 the Tonga-Kermadec Arc, *Global Biogeochem Cy*, 36, e2022GB007363,
1133 <https://doi.org/10.1029/2022GB007363>, 2022.
- 1134 Tomczak, M. and Godfrey, J. S.: *Regional Oceanography: An Introduction*, Daya Publishing
1135 House, 410 pp., ISBN 978-81-7035-306-5, 2003.
- 1136 Tomczak, M. and Hao, D.: Water masses in the thermocline of the coral sea, *Deep-Sea Res*, 36,
1137 1503–1514, [https://doi.org/10.1016/0198-0149\(89\)90054-X](https://doi.org/10.1016/0198-0149(89)90054-X), 1989.
- 1138 Tsuchiya, M.: The Origin of the Pacific Equatorial 13°C Water, *J Phys Oceanogr*, 11, 794–812,
1139 [https://doi.org/10.1175/1520-0485\(1981\)011<0794:TOOTPE>2.0.CO;2](https://doi.org/10.1175/1520-0485(1981)011<0794:TOOTPE>2.0.CO;2), 1981.
- 1140 Tsuchiya, M.: Flow path of the Antarctic Intermediate Water in the western equatorial South
1141 Pacific Ocean, *Deep-Sea Res*, 38, S273–S279, [https://doi.org/10.1016/S0198-0149\(12\)80013-](https://doi.org/10.1016/S0198-0149(12)80013-6)
1142 6, 1991.
- 1143 Tsuchiya, M. and Talley, L.: Water-property distributions along an eastern Pacific
1144 hydrographic section at 135W, *J Mar Res*, 54,
1145 https://elischolar.library.yale.edu/journal_of_marine_research/2191 (last access: 4 March
1146 2024), 1996.
- 1147 Tsuchiya, M., Lukas, R., Fine, R. A., Firing, E., and Lindstrom, E.: Source waters of the Pacific
1148 Equatorial Undercurrent, *Prog Oceanogr*, 23, 101–147, [https://doi.org/10.1016/0079-](https://doi.org/10.1016/0079-6611(89)90012-8)
1149 6611(89)90012-8, 1989.
- 1150 Waeles, M., Baker, A. R., Jickells, T., and Hoogewerff, J.: Global dust teleconnections: aerosol
1151 iron solubility and stable isotope composition, *Environ Chem*, 4, 233,
1152 <https://doi.org/10.1071/EN07013>, 2007.
- 1153 Wilson, E. L., Harpp, K. S., Schwartz, D. M., and Van Kirk, R.: The Geochemical Evolution
1154 of Santa Cruz Island, Galápagos Archipelago, *Front Earth Sci*, 10,
1155 <https://doi.org/10.3389/feart.2022.845544>, 2022.
- 1156 Winckler, G., Anderson, R. F., Jaccard, S. L., and Marcantonio, F.: Ocean dynamics, not dust,
1157 have controlled equatorial Pacific productivity over the past 500,000 years, *P Natl Acad Sci*
1158 *USA*, 113, 6119–6124, <https://doi.org/10.1073/pnas.1600616113>, 2016.
- 1159 Wyrski, K.: The Subsurface Water Masses in the Western South Pacific Ocean, *Mar Freshwater*
1160 *Res*, 13, 18–47, <https://doi.org/10.1071/mf9620018>, 1962.
- 1161 Yeghicheyan, D., Bossy, C., Bouhnik Le Coz, M., Douchet, C., Granier, G., Heimbürger, A.,
1162 Lacan, F., Lanzaova, A., Rousseau, T. C. C., Seidel, J.-L., Tharaud, M., Candaudap, F.,
1163 Chmeleff, J., Cloquet, C., Delpoux, S., Labatut, M., Losno, R., Pradoux, C., Sivry, Y., and
1164 Sonke, J. E.: A Compilation of Silicon, Rare Earth Element and Twenty-One other Trace
1165 Element Concentrations in the Natural River Water Reference Material SLRS-5 (NRC-CNRC),
1166 *Geostand Geoanal Res*, 37, 449–467, <https://doi.org/10.1111/j.1751-908X.2013.00232.x>, 2013.
- 1167 Yeghicheyan, D., Aubert, D., Bouhnik-Le Coz, M., Chmeleff, J., Delpoux, S., Djouaev, I.,
1168 Granier, G., Lacan, F., Piro, J.-L., Rousseau, T., Cloquet, C., Marquet, A., Menniti, C., Pradoux,



- 1169 C., Freydier, R., Vieira da Silva-Filho, E., and Suchorski, K.: A New Interlaboratory
1170 Characterisation of Silicon, Rare Earth Elements and Twenty-Two Other Trace Element
1171 Concentrations in the Natural River Water Certified Reference Material SLRS-6 (NRC-
1172 CNRC), *Geostand Geoanal Res*, 43, 475–496, <https://doi.org/10.1111/ggr.12268>, 2019.
- 1173 Yuan, X. and Talley, L. D.: Shallow Salinity Minima in the North Pacific, *J Phys Oceanogr*,
1174 22, 1302–1316, [https://doi.org/10.1175/1520-0485\(1992\)022<1302:SSMITN>2.0.CO;2](https://doi.org/10.1175/1520-0485(1992)022<1302:SSMITN>2.0.CO;2), 1992.
- 1175 Zheng, L. and Sohrin, Y.: Major lithogenic contributions to the distribution and budget of iron
1176 in the North Pacific Ocean, *Sci Rep*, 9, 11652, <https://doi.org/10.1038/s41598-019-48035-1>,
1177 2019.